

(Univ. Prof. Dr. Friedrich Aumayr)



TECHNISCHE
UNIVERSITÄT
WIEN
Vienna University of Technology



Master Thesis

Ion Guiding Through Insulating Glass Capillaries

Ausgeführt am Institut für
Angewandte Physik
der Technischen Universität Wien
Wiedner Hauptstraße 8-10 / 134
1040 Wien

unter der Anleitung von
Univ. Ass. Dr. Gregor KOWARIK
und
Univ. Prof. Dr. Friedrich AUMAYR

durch
Elisabeth Gruber
Matrikelnummer.: 0625619
Pfeilgasse 3a
1080 Wien

October 25, 2012

(Elisabeth Gruber)

Kurzfassung

Die vorliegende Arbeit beschäftigt sich mit dem sogenannten ‘capillary guiding’ Effekt, der erstmals 2002 in der Literatur erwähnt wird.

Der ‘guiding’ Effekt kann folgendermaßen kurz zusammengefasst werden:

Treffen hoch geladene Teilchen unter einem Kippwinkel auf die Innenseite einer isolierenden Kapillare, werden sie vor dem Auftreffen auf die Oberfläche neutralisiert. Die Nettoladung bleibt an der Oberfläche und wird allmählich durch Ladungstransport abgebaut. Durch die verbleibende Nettoladung wird ein elektrisches Feld aufgebaut, das die nachfolgenden Projektile ablenkt. Daraufhin wechselwirken diese an einer anderen Stelle mit der Oberfläche. Die in einem selbstorganisierenden Prozess entstehenden Ladungsansammlungen führen letztendlich zur Transmission der Projektile durch die Kapillare. Dabei bleibt der ursprüngliche Ladungszustand der einfallenden hoch geladenen Ionen erhalten, was darauf schließen lässt, dass die transmittierten Projektile nie in direkten Kontakt mit der Kapillarinnenoberfläche kommen. Der Kippwinkel ist dabei deutlich größer als der durch die Kapillargeometrie gegebene Transmissionswinkel.

Der erste Teil dieser Arbeit untersucht die Stärke des ‘Guidings’ eines etwa 1 cm langen zylinderförmigen Glasröhrchens mit einem Durchmesser von etwa 100 μm für mehrfach geladene Ar-Ionen in Abhängigkeit vom einfallenden Ionenstrom und der Leitfähigkeit der Kapillare. Letztere kann durch Temperaturänderungen zwischen -25°C und $+90^{\circ}\text{C}$ um mehr als vier Größenordnungen variiert werden. Außerdem wird besonderes Augenmerk auf den transmittierten Ionenstrom bei Temperaturen unter Raumtemperatur gelegt.

Die Messungen zeigen, dass mit ansteigender Temperatur die Stärke des ‘Guidings’ abnimmt und ab Temperaturen oberhalb von etwa 75°C die Transmissionskurve mit der von der Geometrie der Kapillare bestimmten Transmissionkurve zusammenfällt. Dasselbe Verhalten kann durch Verringerung des einfallenden Ionenstrahls bei konstanter Temperatur erreicht werden.

Während bei höheren Temperaturen die Position des transmittierten Ionenstrahls über

Stunden nahezu konstant bleibt, wandert der Strahl bei Temperaturen unterhalb der Raumtemperatur beträchtlich über die Detektorfläche.

Im zweiten Teil wird die gerade verlaufende Kapillare durch eine etwa 5 cm lange konisch verlaufende (Eingangsdurchmesser: $\sim 800 \mu\text{m}$; Ausgangsdurchmesser: $\sim 80 \mu\text{m}$) Glaskapillare ersetzt. Wiederum werden die Auswirkungen der Temperaturänderung zwischen Raumtemperatur und etwa $+90^\circ\text{C}$ auf den 'Guiding' Prozess untersucht. Dabei zeigt sich bei Raumtemperatur ein Einbruch der Transmissionskurve in Geradeausrichtung, der bei geheizter Kapillare nicht mehr beobachtet werden kann. Außerdem zeigt sich, dass im Vergleich zu niederen Temperaturen beträchtlich weniger Ionen durch die Kapillare transmittiert werden.

Abstract

This thesis deals with the so called ‘capillary guiding’ effect, which has been mentioned in the literature for the first time in 2002.

The guiding effect can be described in the following way:

Whenever highly charged ions impinge on an insulating capillary, which is tilted with respect to the beam axis, they become neutralised when hitting the inner surface of the capillary. The deposited charges, which are gradually removed by conductivity, cause an electric field. By this the following projectiles are deflected and interact with the surface at another location. In a self-organized process charge patches are produced and the incoming particles are transmitted through the capillary. The transmitted ions remain in their high charge state, which shows that the projectiles do not get into close contact with the inner wall. Moreover the projectiles are transmitted under angles of incidence much larger than the possible geometric transmission angle, preferentially along the capillary axis (‘guiding’).

The focus of the first part of this thesis lies on the variation of the strength of the guiding of a straight glass capillary (~ 1 cm long, with an inner diameter of about $100 \mu\text{m}$) in dependency of the incoming ion flux and the electrical conductivity of the capillary. The latter can be changed when varying the temperature between -25°C and $+90^\circ\text{C}$ by more than four orders of magnitude. Moreover the transmitted ion beam at very low temperatures is investigated in more detail.

The measurements show, that the increase of the temperature decreases the guiding effect and at temperatures above 75°C the transmission curve corresponds to the geometric transmission through the capillary. The same behaviour is achieved by decreasing the incident ion beam flux at constant temperature.

While at higher temperatures the position of the transmitted ion beam spot is stable over hours, a random motion of the beam spot across the detector can be observed at lower temperatures.

In the second part of this thesis the straight capillary is replaced by a ~ 5 cm long tapered capillary (inlet diameter: ~ 800 μm ; outlet diameter: ~ 80 μm). For this capillary the guiding process is also studied by variation of the sample temperature between room temperature and $+90^\circ\text{C}$. At room temperature a drop of the ion transmission in forward direction is observed, which vanishes at higher temperatures. At the same time a decrease of transmitted ions in forward direction can be noticed in comparison to lower temperatures.

Contents

1	Introduction	8
1.1	Motivation	8
1.2	Capillary guiding	10
1.2.1	First steps	10
1.2.2	A phenomenological description of the guiding effect	12
1.2.3	A theoretical description of the guiding effect	13
1.2.4	Brief historical overview and recent investigations of the guiding effect	16
1.2.5	Applications	22
2	Experimental setup	25
2.1	Ion source	26
2.2	Ion optics	28
2.3	Detection	29
2.4	Data acquisition	32
2.5	Sample holder	34
2.5.1	Sample holder for the straight capillary	34
2.5.2	Sample holder for the tapered capillary	37
2.6	Measuring procedure	44
3	Results	47
3.1	Straight capillary	47

3.1.1	Ion transmission as function of different temperatures and incident ion fluxes	47
3.1.2	Temperature dependent movement of the beam spot on the PSD .	56
3.2	Tapered capillary	60
3.2.1	Guiding effect of tapered capillaries	61
3.2.2	Ion transmission for different temperatures	64
3.2.3	Ion transmission for different incident ion currents	68
3.2.4	Ion transmission for different ion beam energies	68
4	Summary and Outlook	71
4.1	Summary	71
4.2	Outlook	72
	Bibliography	74
	Danksagung	86

1 Introduction

1.1 Motivation

In the last decades a lot of studies on the formation of nanostructures produced at surfaces due to ion impact have been published. Implanting single ions at a desired point on a substrate with nanometer-scale precision could pioneer novel applications as e.g. nano-modifications of surfaces [1–4], fabrication of solid state qubit arrays [5,6] or nano-surgery of living cells [7].

Slow highly charged ions (HCI) are of particular interest due to their high potential energy. When interacting with a surface, HCI deposit their huge potential energy in a small area of a few tens of square nanometers in a very short time (10 fs). Besides the emission of a large number of secondary particles, which enables a detection of each individual ion impact, this causes the formation of well defined single defects on a length-scale of several nanometers. These defects include stable hillocks, pits or crater type nanostructures [3,4,8,9]. The morphology and size of the material modification can be controlled to a certain extent by the charge state of the used incoming ions [10].

The main challenge to define the ion impact point as precisely as possible demands the preparation of a well-focused HCI nano-beam. Therefore, a lot of attention has been paid to linear structures of mesoscopic dimension, such as pores and capillaries. In addition, the fabrication of nano-, micro- and macrocapillaries allows investigations of interaction of HCI with internal surfaces. The so-called capillary guiding effect, which will be described in the next section, could make a tapered capillary a promising candidate for a tool for high-resolution ion beam lithography.

In this master thesis ion guiding through straight and tapered glass capillaries is therefore investigated. The main goal is to control ion guiding through insulating capillaries by changing the electrical conductivity by a few orders of magnitude.

Besides a short historical overview on capillary guiding from its discovery in 2002 to the point of recent investigations, the first chapter of this master thesis gives a phenomenological and theoretical description of the guiding effect.

The experimental setup for macrocapillary guiding is described in chapter 2. Chapter 3 is divided into two parts, whereof section 3.1 presents the experimental results obtained with the straight capillary and section 3.2 the results achieved with the tapered capillary. A summary and outlook is given in chapter 4.

Parts of the master thesis have been submitted for publication in *Physical Review A*¹ and presented as a short oral² and poster contribution³ at the 19th International Workshop on Inelastic Ion-Surface Collisions (IISC-19, Frauenchiemsee/Germany).

¹Gruber,E., Kowarik,G., Ladinig, F., Waclawek,J.P., Schrempf,D., Aumayr,F., Gunacker,P., Schweigler,T., Lemell,C., Burgdörfer,J., 'Temperature Control of Ion Guiding Through Insulating Capillaries', submitted to *Physical Review A* (Sep. 2012).

²Gruber,E., 'Temperature control of ion guiding through straight insulating macro - capillaries', Short oral talk at IISC-19

³(1) G. Kowarik, R. Bereczky, E. Gruber, F. Ladinig, D. Schrempf, P. Gunacker, C. Lemell, J. Burgdörfer, K. Tökési, F. Aumayr, 'Temperature control of ion guiding through straight insulating macro - capillaries', Poster at IISC-19

(2) E. Gruber, P. Hischenhuber, S. Wampl, M. Simon, F. Aumayr, 'Controlling ion guiding through tapered glass - capillaries with temperature', Poster at IISC-19

1.2 Capillary guiding

1.2.1 First steps

In 2002 the capillary guiding effect was mentioned in the literature by Stolterfoht et al. [11] for the first time. The experimental finding was that a beam of HCI in the keV kinetic energy regime can be steered through a thin foil containing insulating nanocapillaries, by tilting the capillary foil with respect to the direction of the incident ion beam. The sample was made of an insulating ~ 10 μm thick PET (polyethylene terephthalate) foil, in which randomly distributed but parallel tracks of swift heavy ions were created by irradiation in an accelerator. These tracks were chemically etched to capillaries of about 100 nm diameter. The front and the back side of the foil was coated with a thin gold layer to avoid charging by the incident ion beam.

The charged particles (Ne^{7+}) were transmitted up to angles of incidence much larger than the possible geometric transmission angle and kept their initial charge-state upon transmission. This was a surprising observation due to the fact, that according to the classical over barrier model (COB), a HCI, which approaches a surface closer than a critical distance of $d \approx \frac{\sqrt{8q+2}}{2W}$ (q denotes the charge state of the incident particle and W the work function of the target), undergoes a neutralisation sequence [12]. This means that the transmitted HCI have been reflected at a distance $D > d$ in front of the surface, probably due to an electric field, caused by the deposited charge of preceding ions.

Some years before, Yamazaki et al [13] have studied the interaction between a HCI beam and an insulator surface of the inner wall of Al_2O_3 -nanocapillaries for the first time. The usage of an additional electron beam avoided any charge-up effects inside the capillary. In this case the charge transfer and the transmission behaviour of the HCIs are the same as in conducting capillaries.

Further experimental work was focused onto metallic multi-capillary foils, instead of insulators [14–18]. This type of foils has been used as a tool for extracting hollow atoms into vacuum and enabled a study of their nature:

According to the COB-model, when HCIs enter the capillary, they are attracted by the image force towards the inner-wall and approach the capillary inner surface. Within a distance less than the critical distance, resonant charge transfer starts. The multiple charged ions capture several electrons from the target into high lying Rydberg-states while the inner shells are left empty. Hollow atoms are formed [12, 19–22]. If the location of the hollow atom formation is close to the exit of the capillary, they are able to escape into the vacuum before hitting the inner wall (figure 1.1). Outside of the capillary the hollow atoms undergo Auger processes and the inner shells are filled again. This has been used to study ‘free’ hollow atoms [23, 24].

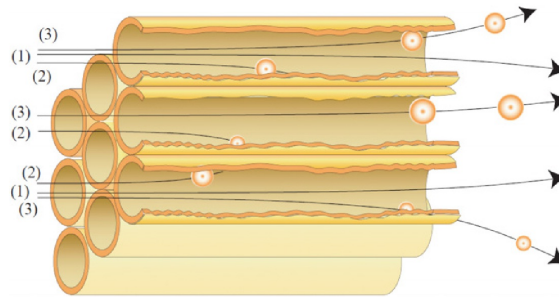


Figure 1.1: **A schematic drawing of the interaction of HCIs in a microcapillary target (taken from [25])**

- (1) The distance of the HCI to the inner-wall is always larger than the critical distance; the HCI passes through the capillary keeping its initial charge.
- (2) When the distance becomes shorter than the critical distance, hollow atoms are formed and then hit the inner wall.
- (3) The location of the formation of hollow atoms is close to the exit of the capillary and the hollow atoms can escape into vacuum before hitting the surface.

Afterwards, insulator multi-capillary foils were investigated by Stolterfoht et al. This was the starting point for detailed investigations of the capillary guiding phenomena for various materials, projectiles and geometries (for a short review see e.g. [25]). Before

giving a short historical overview on the processing of the last decade, a phenomenological and theoretical description of the guiding effect is given in the next two sections.

1.2.2 A phenomenological description of the guiding effect

The guiding effect inside an insulating capillary is tentatively explained as the consequence of a self-organized formation of charged areas inside the capillary, which deflect succeeding ions and eventually guide them through the capillary. After some irradiation time a dynamical equilibrium of charging-up, charge relaxation and reflection is established and stable transmission is observed. The fact that the transmitted ions keep their charge-state confirms the assumption that the particles are guided through the capillary without getting into close contact with the capillaries' walls; the transmitted particles are reflected in front of the surface due to an electric field, caused by the deposited charge of the preceding ions.

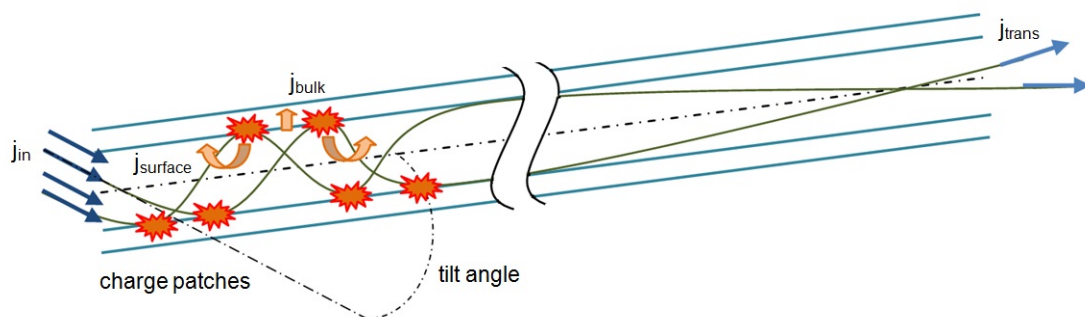


Figure 1.2: A phenomenological picture of the guiding effect

The incident ion beam (flux j_{in}) hits the wall close to the entrance and creates charge patches. Charge transport allows an electrical current into the bulk (j_{bulk}) and along the surface ($j_{surface}$). The succeeding ions are deflected by the evolving electric field and create a second charge-patch at another location or are transmitted through the whole capillary. A number of charge-patches can be created along the inner wall of the capillary sample to establish the guiding field.

A simplified picture of the guiding process inside a capillary is described in the following (figure 1.2): The incoming ion beam gets into close contact with the capillary's inner wall of the entrance and undergoes a neutralisation sequence. The electrons are captured from a small vicinity around the impact location and the first charge-patch is created. The succeeding ions are deflected by the evolving electric field and create a second charge-patch at another location or are transmitted through the whole capillary. A number of charge-patches evolve along the sample and create a guiding field. As soon as the charge distribution along the capillary reaches a dynamic equilibrium between conduction losses and impinging projectiles, a stable ion transmission is reached.

It was found experimentally that the time-evolution of the ion transmission can be described quite well by a $1 - e^{-\frac{t}{\tau_1}}$ law ($\tau_1 \approx 2.5$ min) for the charging period, while the descent $\sim e^{-\frac{t}{\tau_2}}$ of the transmission due to discharging proceeds with a larger time constant $\tau_2 \approx 40$ min [11].

1.2.3 A theoretical description of the guiding effect

A theoretical description and simulation of the guiding process is a considerable challenge in view of the widely disparate time scales: the microscopic charge-up by HCIs takes place on a fs time scale, the transmission time of a projectile ion through the capillary on a ns scale and the diffusive rearrangement of charges and the discharging on a macroscopic time scale (> seconds).

During the past years simulations about the guiding through nanocapillaries were carried out [26–31]. These simulations could reproduce a range of the first experimental findings, e.g. ion guiding even for large incidence angles, the temporal increase/decrease of transmission during beam-on/beam-off times and, in part, a relatively large angular spread of the transmitted beam. The model for these simulations represented a mean-field classical transport theory based on a microscopic classical trajectory Monte Carlo simulation for the ion transport, self-consistently coupled to the charge-up of and charge diffusion near the internal capillary walls [28].

As a limiting case Schiessl et al. [26] consider also a simplified rate-equation approach, which shows partial agreement with the experimental data.

The balance equation for the deposited charge $q_S(t)$ at the surface of the capillary reads

$$\frac{dq_S(t)}{dt} = j_{in} - j_{tr} - j_S \quad (1.1)$$

where j_{in} is the incident current, j_{tr} the transmitted current and j_S the current absorbed in the capillary surface. The latter includes the current into the bulk and the current along the surface.

$$j_S = \left(\frac{1}{\tau_s} + \frac{1}{\tau_b} \right) q_S = \frac{q_S}{\tau_{eff}} \quad (1.2)$$

The solution of equation (1.1) corresponds well with the experimental observed evolution of the transmission during the charging period for switch-on with the initial condition $q_S(t=0) = 0$

$$q_S(t) = \tau(j_{in} - j_{tr})(1 - e^{-t/\tau_{eff}}) \quad (1.3)$$

and for the switch-off at $t = t_0$

$$q_S(t) = q_S(t_0)e^{-t/\tau_{eff}} \quad (1.4)$$

Taking also the bulk charge $q_b(t)$ into account, the total charge determines the transmission

$$q(t) = q_b(t) + q_S(t) = q_0 \left[C e^{-t/\tau_b} + (1 - C) e^{-t/\tau_{eff}} \right] \quad (1.5)$$

with $C(q_S, \tau_S, \tau_b) < 1$.

For the case of capillaries in a PET-foil, $\tau_S \ll \tau_b$ and therefore, the transmission drops fast in the beginning and becomes then a slowly decaying function. In contrast to PET-foils, for the glass capillaries the approximation of $\tau_S \ll \tau_b$ is no more valid.

While the guiding process for nanocapillaries can be simulated, Monte Carlo simulations for macroscopic capillaries are out of reach considering current computational capabilities. Instead, a simplified rate equation model for the first and dominant charge patch, which is assumed to be primarily responsible for establishing stable guiding conditions, was developed [32]. An important difference between glass capillaries and the

previous simulated nanocapillaries is the minor importance of the surface conduction in comparison to the now dominant bulk conduction.

The rate equation model presented before, which has been validated by microscopic transport simulations for nanocapillaries, was extended to the following balance equation for the deposited charge in the primary patch $Q_p(t)$

$$\frac{dQ_p(t)}{dt} = \left(j_{in} - j_{tr} - j_d - \frac{Q_p(t)}{\tau} \right) - \left(\frac{dQ_p}{dt} \right)_{stoc} \quad (1.6)$$

where again j_{in} is the incoming ion current, j_{tr} the current transmitted through the capillary and j_d the current of deflected projectiles eventually forming subsequent patches downstream [32]. The stochastic non-linear discharge term dQ_p/dt is in general a functional of the charging history and contributes to the process above a critical value. This term is neglected when a unique stable dynamical equilibrium is reached, but becomes important for the description of non-steady states.

Again the adsorption into the wall is split into two components, one depends on the surface diffusion j_s and the other on the bulk conductivity j_b .

$$j_p = j_s + j_b$$

with the effective discharge time

$$\tau = \left(\frac{1}{\tau_s} + \frac{1}{\tau_b} \right)^{-1}$$

The discharge time τ is directly related to the conductivity $\sigma(T)$ by $\tau^{-1} \sim \sigma(T)$ and therefore strongly dependent on the temperature T (\rightarrow figure 3.1 in chapter 3).

Under equilibrium conditions $\left(\frac{dQ_p(t)}{dt} = 0 \right)$ j_d is negligible and j_{tr} becomes proportional to j_{in}

$$j_{tr} = f(Q_p, \phi, E, T) j_{in} \quad (1.7)$$

where f denotes the fraction of transmitted ions, depending on the accumulated charge Q_p , the capillary tilt angle ϕ , the energy E of the incident particles and the temperature T .

With eq. (1.6) and (1.7), the equilibrium charge is given by

$$Q_P = j_{in} \tau (1 - f(Q_P, \phi, E, T)) \quad (1.8)$$

When neglecting the dependence of f on Q_p , equation (1.8) predicts that Q_p becomes proportional to the product of incident current and discharge time:

$$Q_p \propto j_{in} \tau(T) \propto \frac{j_{in}}{\sigma(T)} \quad (1.9)$$

Keeping the incident current constant while increasing the temperature (i.e. the conductivity) will lead to a lower equilibrium value for the total charge Q_p and consequently a reduction of the transmitted particle flux j_{tr} . The same effect can be achieved by keeping the temperature constant while reducing the incident ion flux.

1.2.4 Brief historical overview and recent investigations of the guiding effect

After the guiding effect has emerged, the ‘guiding power’ has been introduced to quantitatively characterise the ‘strength’ of the effect. The ‘guiding power’ ϕ_c is a measure for the width of the Gaussian fit through the measured transmission intensity as a function of the capillary tilt angle ϕ [11].

$$I(\phi) = I(\phi = 0) \cdot e^{-\frac{\sin^2 \phi}{\sin^2 \phi_c}} \quad (1.10)$$

or approximately

$$I(\phi) = I(\phi = 0) \cdot e^{-\frac{\phi^2}{\phi_c^2}} \quad (1.11)$$

for small tilt angles.

ϕ_c is also called the ‘guiding angle’ and is determined by the $1/e$ drop of the intensity.

The guiding power can be influenced by several conditions. Thus, material properties highly influence the guiding effect and have been investigated in several experiments. In the beginning measurements with randomly distributed and parallel nanocapillaries in PET foils [11, 33–41] were performed (left figure of 1.3). The development of the fabrication of regular arrays of well aligned nanocapillaries in SiO₂ [42] allowed the studies of guiding properties as well in these materials [43–45] (right figure of 1.3).

In addition, the guiding effect has been studied also in nanoscale apertures in silicon nitride membranes [46] as well as in Al_2O_3 [47–51].

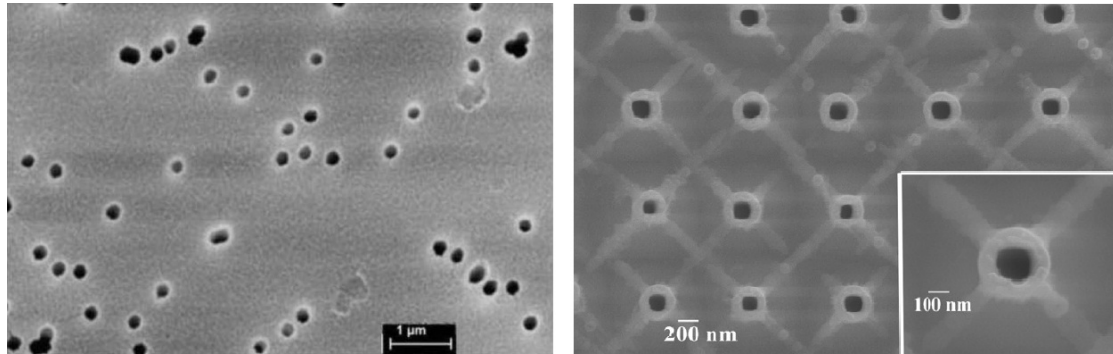


Figure 1.3: **View of randomly and regularly distributed nano-capillaries**

left: Randomly distributed nano-capillaries in a PET foil [52]

right: Regular array of SiO_2 nano-capillaries [42]

Further parameters, which influence the guiding power, are the charge state and the energy of the projectiles. References [52–54] present systematic studies of the width of the transmitted profile as well as the guiding power by varying these two parameters. The scaling law describes the dependence of the ion transmission on tilt angle, energy and charge state of the incident HCl. The major parameter for scaling is E_{kin}/q and determines $1/\sin^2 \sigma_t$ and $1/\sin^2 \phi_c$ in a slightly non-linear way (see figure 1.4).

Moreover, the guiding effect was also studied for various capillary geometries. The guiding ability doesn't change significantly when increasing the nanocapillary diameter from 100 nm to 400 nm [55] and works also on a macroscopic length-scale. This was demonstrated firstly with a single large tapered capillary (length: 5 cm, inlet diameter: 0.8 mm, outlet diameter: 24 μm) [56] and then also with a single macroscopic straight glass capillary (length: 5 cm, diameter: 0.12 mm) at TU Wien [57, 58].

Besides that, capillaries with cross sections other than circular ones were recently studied. So the references [59, 60] present the guiding of ions through rhombic nanocapillaries and [61] through rhombic and rectangular nanocapillaries. In these the unexpected effect

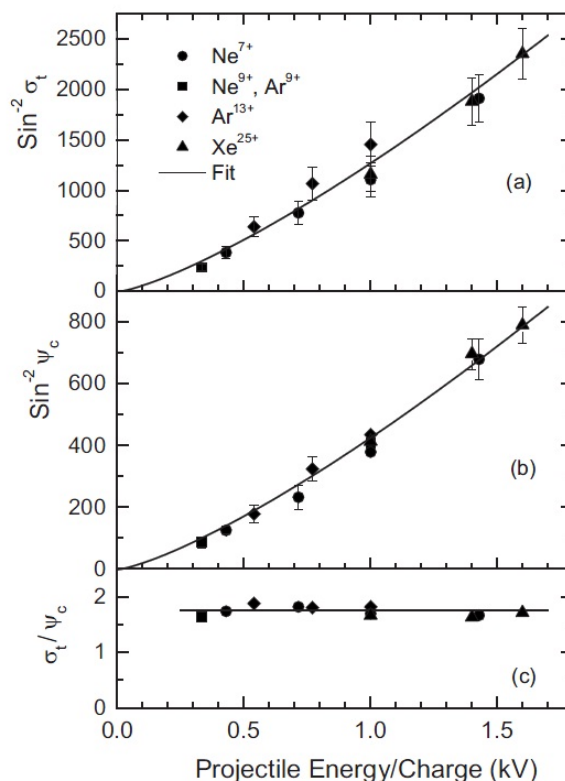


Figure 1.4: **Scaling laws for the width σ_t (FWHM) of the transmission profile and the guiding angle ϕ_c ($= \psi_c$ in this figure) taken from [52]**

was found, that capillaries of rhombic cross section produce rectangular shaped ion transmission profiles and vice versa (see figure 1.5). The authors explain these experimental findings (supported by associated simulations) as a result of image forces experienced by the transmitting ions.

Furthermore, ion beam guiding has been studied with straight and curved Teflon tubes [62]. The guiding capability was tested for several bending angles (9.6° , 17.5° and 26.7°) and a transmission efficiency of Ar^{8+} ions of several tens per cent could be detected. It turned out, that the beam-guidable bending angles of the curved Teflon tubes are much larger than the limit guiding angle with the straight tube of the same size. This may open a way of flexible ion beam deflector systems similar to fibre optic guides.

Besides the guiding of HCIs through capillaries, also the so-called double ion guiding of

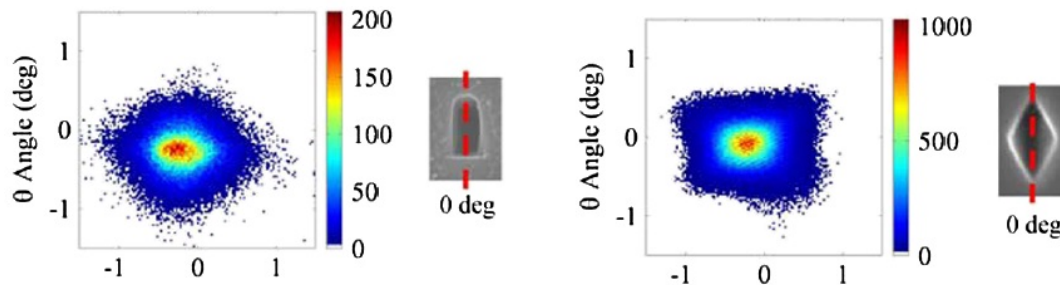


Figure 1.5: **2D angular distribution for 7 keV Ne^{7+} ions transmitted through capillaries of rectangular (left) and rhombic (right) cross sections [61].**

ions between a set of two parallel plates was studied in the last years [63–65]. The double ion guiding describes the effect, that the beam deviates in the plane of the capillary plates when the glass plates are turned round an axis perpendicular to them. This effect can be explained by the formation of a conductive channel on each of the two glass plates, which causes a guiding electrical field.

While for HCIs the guiding through insulating capillaries was observed, electrons are also deflected by using similar interaction geometries. Milosavljević et al. [66] present the transmission of electrons (initial energy of about 200-350 eV) through Al_2O_3 capillaries under tilt angles of several degrees. The measurements [67, 68] show the massive energy loss of electrons after the interaction with tilted nanocapillaries, which can be understood by multiple inelastic scattering events with the surface, and give an explanation for the transmission of electrons through insulating capillaries at tilt angles larger than the geometric opening angle. It's still an open question which role the guiding effect has for the transmission of electrons, as there also seem to be some time dependent phenomena [69, 70]. An additional point, which has to be considered, is the production of secondary electrons, which were also measured behind the sample [71]. Simulations about electron transmission through insulating nanocapillaries can be found in [72].

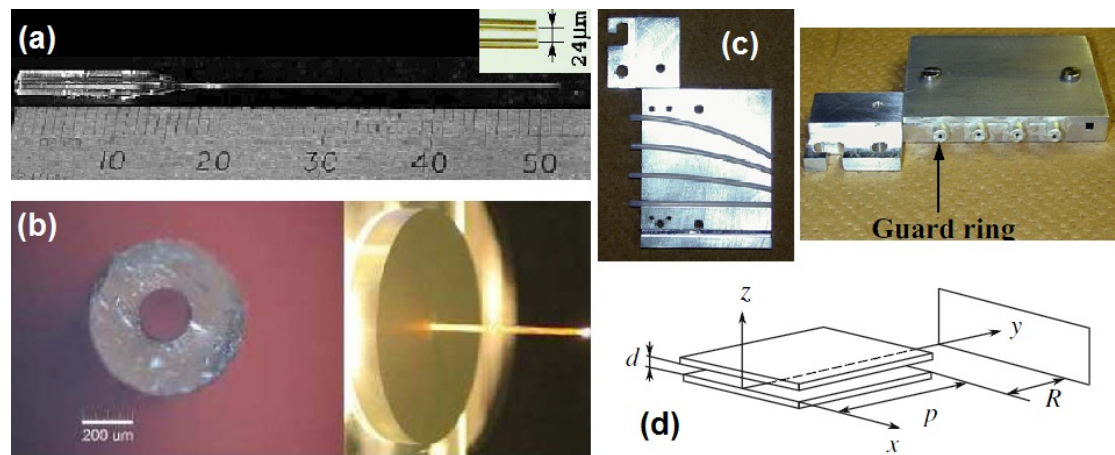


Figure 1.6: **Various macroscopic geometries**

- (a) Picture of a tapered glass capillary [56]
- (b) Pictures of a straight glass capillary [58]
- (c) Picture of straight and curved Teflon tubes [62]
- (d) Schematic drawing of capillary plates [63]

The scattering rather than the guiding effect dominates also the transmission of swift highly charged ions (MeV energies) through capillaries [73].

In addition to positive ions and electrons, also more ‘exotic’ projectiles, like negative ions [51, 74–77], positrons [78, 79] and muons [80, 81] were used to study the interaction with insulating capillaries.

One of the key parameters for controlling the ion guiding through insulating capillaries is the electrical conductivity. Kowarik et al. [82, 83] started to investigate the guiding effect by varying the electrical conductivity by changing the capillary’s temperature. The measurements have been performed with a single straight macroscopic glass capillary. The results have been confirmed and extended during the course of this master thesis and are presented in the following chapters in more detail.

The temperature control of ion guiding was also studied for a macroscopic tapered glass capillary during this master thesis. As just mentioned before, tapered capillaries are possibly promising tools for future surface lithography by slow HCIs and investigated by various experimental groups. So Ikeda et al. [56] show besides the guiding also a focusing effect for tapered capillaries; the beam density was enhanced as compared to the freely traveling beam. The guiding and focusing effect of tapered capillaries was also observed for higher charge-states (230 keV Xe²³⁺) [84].

Another interesting experimental observation when using tapered capillaries has been described in [85]. There Kreller et al. find a considerable suppression of the transmitted ions in forward direction at room temperature. One possible explanation for this behaviour would be, that a uniformly charged ring-shaped region in the tapered part of the capillary causes the blocking.

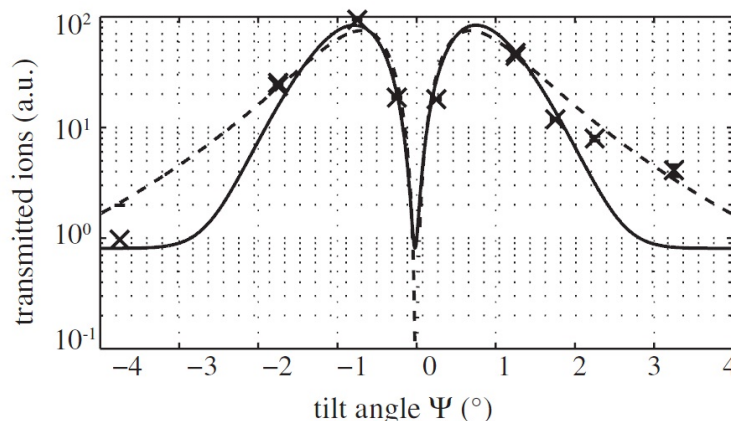


Figure 1.7: **Measured transmission curve with suppression in forward direction from the literature [85]**

Transmission of Ar⁸⁺-ions at a kinetic energy of 24 keV. The solid line indicates the fit of the measured data to eq. (1.12) and the dashed line to eq. (1.13).

In figure 1.7 the respective transmission yield depending on the tilt angle is fitted by the following functions, one based on a Gaussian ansatz and the other on a square-Lorentzian ansatz ($\phi_{C,G}$ guiding angle for the Gaussian ansatz; $\phi_{C,S}$ guiding angle for

the square-Lorentzian ansatz; $F_{0,G/S}$ and $\phi_{sup,G/S}$ parameters for power and width of the suppression)

$$f_G(\phi) = f(0) \cdot \left(e^{-\frac{\sin^2 \phi}{\sin^2 \phi_{C,G}}} - F_{0,G} \cdot e^{-\frac{\sin^2 \phi}{\sin^2 \phi_{sup,G}}} \right) \quad (1.12)$$

$$f_S(\phi) = f(0) \cdot \left(\left(1 + \left(\frac{\phi}{\phi_{C,S}} \right)^2 \right)^{-2} - F_{0,S} \cdot \left(1 + \left(\frac{\phi}{\phi_{sup,S}} \right)^2 \right)^{-2} \right) \quad (1.13)$$

Such a blocking effect in a macroscopic tapered capillary has been mentioned before by Nakayama et al. [86] (figure 1.8) using ions at very high charge state ($10 \leq q \leq 50$). Steady transmission state could be found for preferable angles and blocking at smaller angles.

In the following chapters the focus lies also on this ‘blocking’ effect. The ambition is to check if the predicted ‘suppression’ of the transmitted ions in forward direction at room temperature can be reproduced and if this drop in can be terminated by an increase of the capillary temperature.

1.2.5 Applications

Before discussing the experimental setup and results of the measurements in detail, a short overview on possible applications of guiding through insulating capillaries in the last years is given.

In [87] Nebiki et al. present a novel technique to introduce high energy ion beams (MeV) to atmospheric environment, which enables in-air PIXE (particle induced X-ray emission) measurements. In this case a slightly tapered capillary works as a differential pumping orifice as well as a focusing lens. References [88, 89] describe the usage of a tapered glass capillary tube for beam focusing in a compact micro-PIXE system. In reference [88] a micro-beam of swift protons, transported through a tapered capillary, irradiates a thin metallic foil and produces quasi-monochromatic X-rays, which can then be used for

high-contrast radiography.

Further applications can be found for in-air STIM (scanning transmission ion microscopy) [90]. There, a tapered glass micro-capillary is used to collimate a MeV ion beam to a diameter of approximately 1 μm without any other ion optical lenses. The collimated beam can be taken into air without any membrane or special differential pumping, due to the small gas leakage through the capillary opening and used in the following for STIM measurements.

The usage of tapered capillaries as a facility to collimate a particle beam down to some μm sized beam spots, has found its application also for a micro-beam NRA (nuclear reaction analysis) system for the purpose of the 3D mapping of the hydrogen distribution in solids [91].

Tapered capillaries with a thin window at the tip are a promising tool for novel analysis, radiation testing and surface modification processes. In [92], for example, polyethylene and polytetrafluoroethylene are irradiated with H^+ ions in an aqueous solution containing acrylic acid monomers. The originally hydrophobic surface becomes by irradiation hydrophilic.

A further example is given in [93], where energetic ions are injected into a cell through a tapered capillary with a thin window at the outlet, involving selective inactivation or disruption of cellular structures.

Tapered capillaries used for surface modifications and as biological tools are also described in [94].

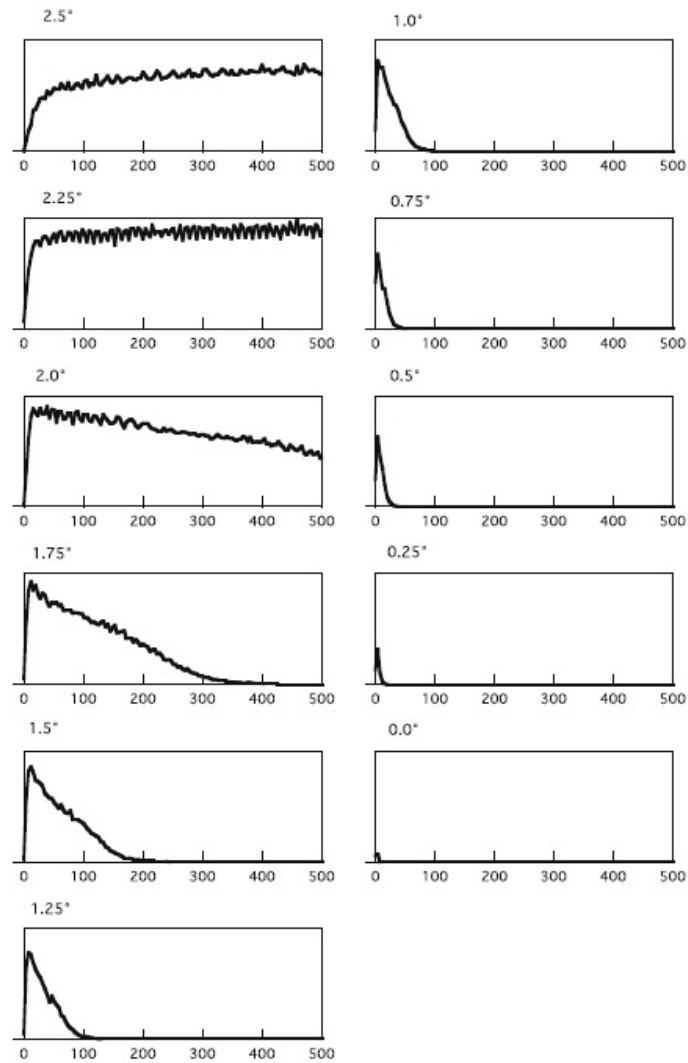


Figure 1.8: **Guiding and blocking of highly charged ions through a tapered capillary [86]**

Transmission of highly charged ions as a function of capillary tilt angle (vertical axes: transmitted ions at the same scale; horizontal axes: time in seconds).

2 Experimental setup

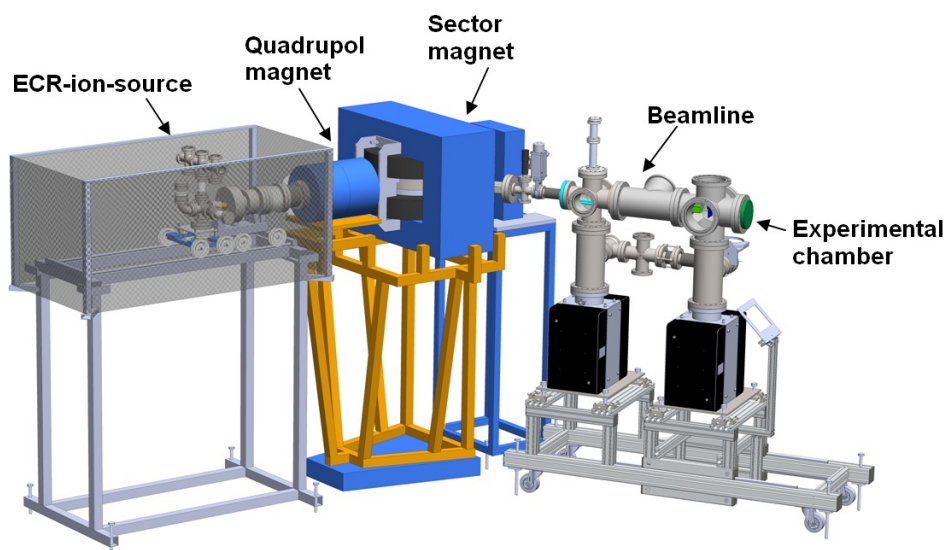


Figure 2.1: Schematic drawing of the ion beam facility at TU Wien, taken from [95]

The experimental setup consists of an ECR-ion source for the production of slow, singly and multiply charged ions, two magnetic quadrupole lenses for focusing and a sector magnet for mass-to-charge separation of the ion beam. After entering a differentially pumped beamline, the ions are guided into the experimental chamber, where the capillary holder and a position sensitive detector (PSD) are placed.

2.1 Ion source

The slow, singly and multiply charged ions are produced by an all-permanent-magnet electron cyclotron resonance ion source (ECRIS) at the Institute of Applied Physics at TU Wien [96]. The source is capable of producing ions at extraction voltages up to 6 kV and at charge states up to Ar^{11+} .

In a plasma chamber the highly charged ions are produced by step-by-step ionization induced by electron-impact. The plasma is confined by the magnetic field of four permanent magnet rings and a Halbach-type hexapole magnet.

The electrons are heated resonantly by microwave radiation. The microwaves are generated by a thin film oscillator in the range between 12.75 GHz and 14.5 GHz, amplified by a microwave amplifier and transported into the main source chamber through a Polytetrafluoroethylene window, which also provides isolation of the source chamber.

Two separated gas inlet valves enable a mixture of gases in the plasma chamber. This can be beneficial for the production of highly charged ions.

The ions are extracted from the plasma using an ‘accel-decel’ extraction system, consisting of three barrels (figure 2.2); the one which is turned toward the source main chamber is on source potential, the next can work as a suppressor electrode and the last one is on ground potential. The positively charged ion beam is accelerated from the positive plasma potential to the ground potential. This extraction voltage, multiplied by the ion charge state, determines the kinetic energy of the ion beam.

Afterwards the ions pass two magnetic quadrupole lenses, one focussing the beam in the vertical plane and the other in the horizontal. In the following magnetic sector field the ions are mass-to-charge separated and then guided into one of the three beamlines.

The operating parameters for the ECR-ions source, the quadrupole magnets and the sector magnet are computer controlled and monitored by a LabVIEW program [97]. The

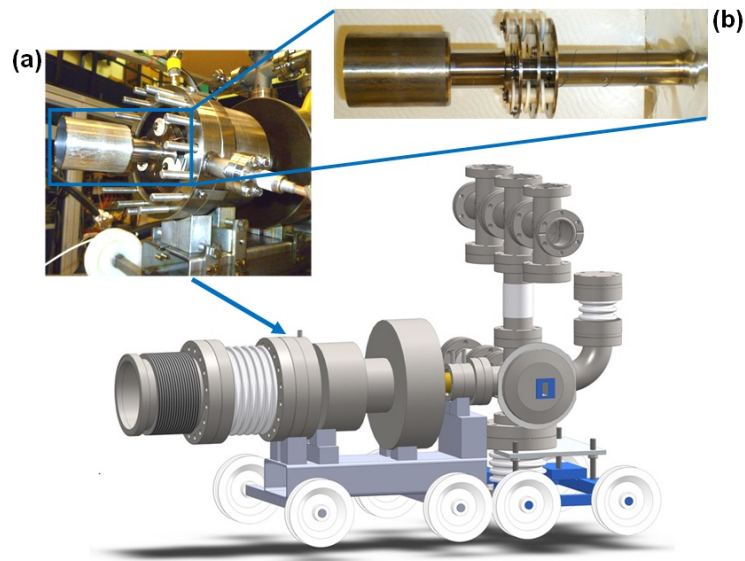


Figure 2.2: **Schematic view of the ECR-ion-source SOPHIE**

The two images (a) and (b) show the extraction system of the ion source. It consists of three barrels which are isolated from each other. The one which is turned towards the source main chamber is on source potential, the second can work as suppressor electrode and the last one is kept on ground potential.

vacuum system is fully controlled and automated by a programmable logic controller (PLC), which also monitors the cooling water feed for the magnets [98,99].

The ECRIS, quadrupoles and sector magnets are separated from the three beamlines by pneumatically operating shutters. Between the sector magnets and the shutters, Faraday cups on pneumatic manipulators enable the measuring of the spectra of the extracted ions.

The presented measurements were performed with Ar^{q+} -ions at a charge-state of $7 \leq q \leq 9$ and with kinetic energies between 4.5 keV and 16 keV.

2.2 Ion optics

The ion optical system consists of a collimator and a lens system with several sets of deflection plates and apertures for guiding the ion beam into the experimental chamber. An electrostatic einzel-lens can be used to further focussing of the ion beam.

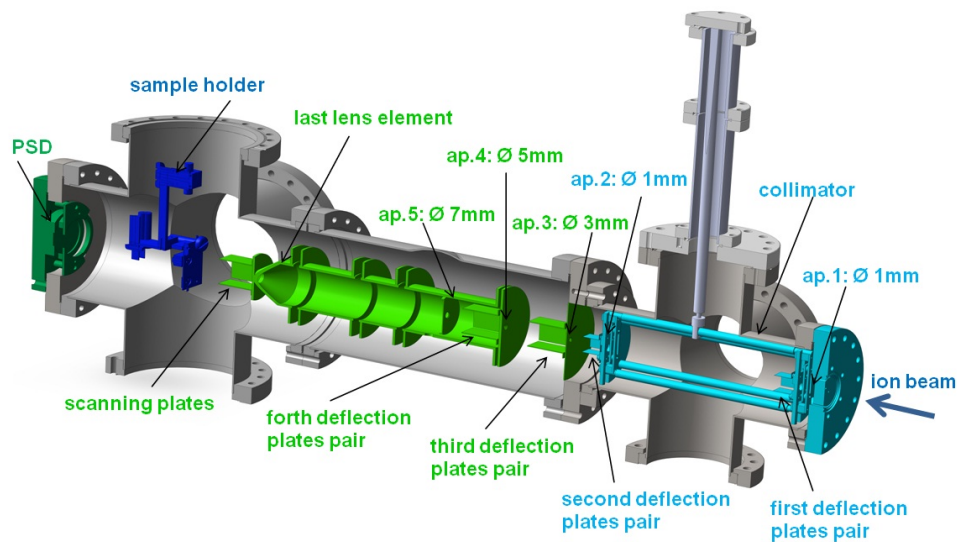


Figure 2.3: **View of the ion optical system**

The ion optical system consists of a collimator and a lens system with several sets of deflection plates and apertures for guiding the ion beam into the experimental chamber. The electrostatic lens can be used for focusing.

The measurements are performed by using the collimator-apertures of 1 mm diameter, which enables a maximum opening angle of approximately $\pm 0.5^\circ$ of the ion beam.

At first the ion beam crosses the collimator, consisting of two sets of apertures of different diameters (250 μm , 500 μm , 1 mm, 3 mm, >3 mm), which are mounted on a sliding carriage in a distance of 230 mm. A set of deflection plates between these two sets are used, to guide the ion beam through the collimator.

The presented measurements are performed by using the 1 mm apertures, estimating a maximum opening angle of the ion beam of approximately $\pm 0.5^\circ$.

Afterwards two grounded apertures (diameter of 2 mm) in front of the first and after the second aperture of the collimator had to be added, preventing that the incident beam accidentally passes through two apertures of different diameters of the collimator.

The collimated beam travels a distance of about 0.5 m until it reaches the capillary's entrance. In this drift region an electrostatic lens can be used for focussing the beam, but usually isn't operated in order to preserve the specified geometric opening angle. Three sets of deflection plates, located in this lens system, are used to guide the particle beam into the experimental chamber. The diameter of the beam spot, which finally hits the capillary entrance, is about 3 mm.

The deflection plates directly in front of the capillary entrance can be used to influence the direction of the ion beam, hitting the capillary's entrance. During most of the measurements these plates are grounded.

Primarily these deflection plates are used as scanning plates for calibration purpose; the ion beam is scanned across the whole active area of the MCP detector (see section 2.3).

2.3 Detection

Besides the capillary holder, the experimental chamber contains a position sensitive detector at the backside flange for recording the impinging particles.

The detector consists of a set of micro-channel-plates (MCP) in chevron configuration in front of a wedge-and-strip-anode [100] (figure 2.4). The MCP has to be operated with a voltage difference of 1.5 kV to 2.2 kV between the MCP-front and backside. A germanium-layer between the MCP and the anode, which is kept about 50 V to 100 V more positive than the MCP's backside, enables the operation of the preamplifier, and therefore of the anodes, on ground potential.

The voltage difference of ~ 1.7 kV between the front and backside of the MCP can be achieved by keeping the front on high negative voltage (-1.7 kV to -2 kV) and the backside close to ground potential and therefore close to the voltage of the preamplifier.

2 Experimental setup

This operating mode is indeed safer for the electronics, however, the ions are highly deflected by the strong electric field in front of the detector and the imaging quality is poor. For this reason the presented measurements are performed by keeping the MCP's frontside on -150 V and the backside between 1.5 kV to 1.6 kV. The voltage of -150 V on the frontside is low enough not to influence the trajectories of the incident ions significantly and, on the other hand, high enough to prevent counting parasitic electrons.

When the incident ions hit the MCP, electrons are emitted, which are then accelerated and multiplied in the electrical field between the front- and the backside of the MCP. Afterwards the multiplied electrons are accelerated towards the germanium layer and the image charges of the electron cloud produce a signal at the wedge-and-strip-anode.

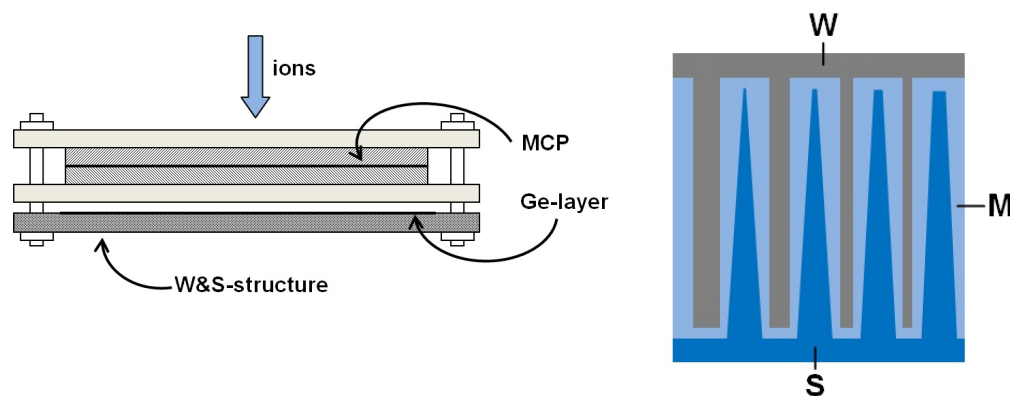


Figure 2.4: **Schematic drawing of the position sensitive detector assembly and a schematic view of the wedge-and strip anode**

left: Schematic view of the assembling of the position sensitive detector

right: The lateral position of the electron cloud can be extracted from the pulse-heights of three signals of the special shaped anodes (wedge (W), strip (S), meander (M))

The lateral position of the electron cloud on the detector can be extracted from the

2 Experimental setup

pulse-heights of three signals of the special shaped anodes (wedge, strip, meander).

The fraction between the three signals of one event produces a 2-dimensional picture.

The meander-electrode is used to normalise the signals to the total deposited charge. The x-and y- coordinates are calculated by the following law:

$$x = \frac{Q_W}{Q_W + Q_S + Q_M} \quad (2.1)$$

$$y = \frac{Q_S}{Q_W + Q_S + Q_M} \quad (2.2)$$

The measured values for the deposited charges at the wedge- (Q_W), strip- (Q_S) and meander-anode (Q_M) have to be scaled by a factor, which takes the different amplification into account. The calibration factors are found by scanning the ion beam across the whole detector and optimizing the observed 2D-shape to be circular with a diameter of 47 mm. In addition the calibrated linear coordinates are rotation-transformed and mirrored to take the detector's orientation into account.

$$x = scal \cdot \left[\cos(cal_\phi) \cdot \left(\frac{cal_1 \cdot Q_W}{cal_1 \cdot Q_W + cal_2 \cdot Q_S + cal_3 \cdot Q_M} - cal_x \right) + \sin(cal_\phi) \cdot \left(\frac{cal_2 \cdot Q_S}{cal_1 \cdot Q_W + cal_2 \cdot Q_S + cal_3 \cdot Q_M} - cal_y \right) \right] \quad (2.3)$$

$$y = scal \cdot \left[\cos(cal_\phi) \cdot \left(\frac{cal_2 \cdot Q_S}{cal_1 \cdot Q_W + cal_2 \cdot Q_S + cal_3 \cdot Q_M} - cal_x \right) - \sin(cal_\phi) \cdot \left(\frac{cal_1 \cdot Q_W}{cal_1 \cdot Q_W + cal_2 \cdot Q_S + cal_3 \cdot Q_M} - cal_y \right) \right] \quad (2.4)$$

$cal_{1/2/3}$...calibration factors of the three anodes for taking the different amplification into account

$cal_{x/y}$...correction factors for shifting the centre of the detector into the (0/0) position

cal_ϕ ...correction factors for rotation calibration

$scal$...scaling factor

2.4 Data acquisition

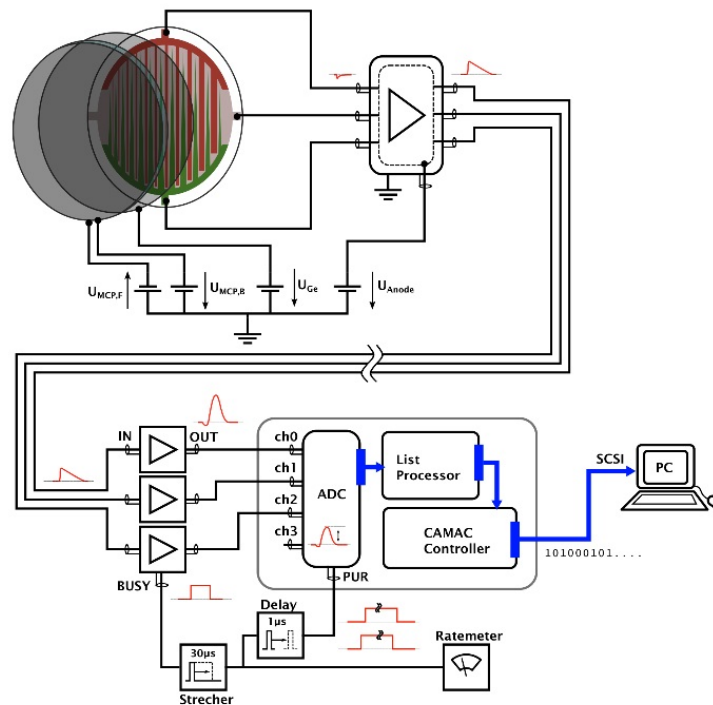


Figure 2.5: **Schematic view of the position sensitive detector wiring and the data acquisition system (figure from [82])**

The wedge-and-strip-anode provides three signals for each event, which are preamplified by the Roentdek 3-channel-preamplifier and then sent to three Ortec 570 amplifiers. The amplified pulses are sequentially digitised by a four-parameter analogue-to-digital-converter (ADC).

An event is triggered by the busy-signal of the meander channel's amplifier. Everytime the signal exceeds a lower level, the amplifier sends a TTL pulse to the ADC's master-gate-input to trigger a conversion. The ADC is located in a CAMAC crate (Sparrow MINICRATE Model 1000) together with a list processor (Hytec LP1342) and a suitable CAMAC controller (Sparrow Model 73A). After a conversion, the ADC triggers an interrupt at the list processor and the digitised values are written into a buffer memory.

2 Experimental setup

This transfer takes about 25 μs . To prevent that subsequent events invalidate the data, an artificial dead time τ_D (busy pulse is stretched to a length of 30 μs and shifted by 1,5 μs) is introduced. As any event occurring during this time is not recorded, the measured rate has to be corrected afterwards. The relation between the actual count rate R and the measured rate $R_{measured}$ is the following¹

$$R = \frac{R_{measured}}{1 - (\tau + \tau_D)R_{measured}} \quad \Leftrightarrow \quad R_{measured} = \frac{R}{1 + (\tau + \tau_D)R} \quad (2.5)$$

As soon as the buffer memory exceeds 5.000 events, the data is sent via a SCSI bus line to the connected PC and recorded by the software tool KMax 7.1 [101] (figure 2.5).

In order to get a timestamp to each event, a short and a long-term timescale are used. The long-term one uses the computer clock to synchronise the events between two subsequent transfers from the CAMAC to the PC, having a whole buffer set of 5.000 events at the same time. The short-term timescale uses a timer at a fixed frequency that writes every 6 ms an artificial event timer into the buffer.

When a real event is being processed, the list processor ignores the trigger used for the timestamp-events and the timestamp is lost. For this reason the previously given equation 2.5 has to be slightly modified to (figure 2.6):

$$R_{measured} = \frac{\frac{R}{1 + (\tau + \tau_D)R}}{1 + \tau_{trigger} \frac{R}{1 + (\tau + \tau_D)R}} = \frac{R}{1 + (\tau + \tau_D + \tau_{trigger})R} \quad (2.6)$$

The whole buffer set is transferred to the PC and written into an event-file. The produced ASCII-files are evaluated by the IGOR Pro data acquisition and analysis software [102].

¹The actual impingement rate based on the measured rate is calculated under the assumption of the underlying Poisson statistics. τ is the mean waiting time between two subsequent events to occur. For further explanation see [82]

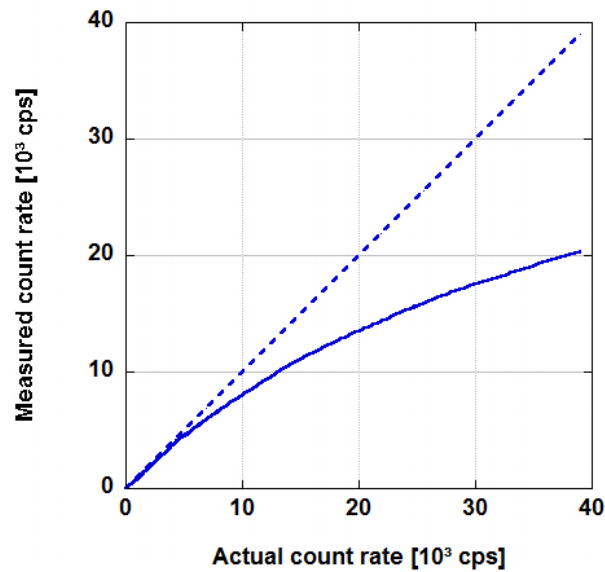


Figure 2.6: **Corrected count rate curve** (from [82])

The solid line shows the proposed correction of eq. (2.6) of the measured rate as a function of the real impingement rate. The dashed line shows the ideal case.

2.5 Sample holder

The sample holder is located in the experimental chamber about 180 mm in front of the PSD. The experimental chamber is kept under UHV conditions at a base pressure below 1×10^{-9} mbar. The sample holder is mounted on the rotatable rod of a 3-axis manipulator. The movement of the holder is stepper motor driven with a relative position accuracy of $20 \mu\text{m}$ in x, y and z-direction and an angular resolution of 0.01° .

2.5.1 Sample holder for the straight capillary

The first measurements are performed by using a single straight glass capillary. It is made of borosilicate glass (trademark Duran) and was fabricated at the Institute of Nuclear Research of the Hungarian Academy of Sciences.

Kowarik et al. [57, 58, 82, 103] could demonstrate the guiding effect for this insulating capillary with macroscopic dimensions of 11.4 mm length and an inner diameter of 140 μm and started to investigate in more detail how a variation of the electrical conductivity influences the guiding power.

For these measurements a capillary holder was constructed, which enables a temperature variation of the capillary between -35°C and $+90^\circ\text{C}$. This experimental setup is also used for the first measurements performed during this master thesis and is therefore shortly presented in the following paragraph. Further details can be found in [82].

The straight glass capillary is sandwiched between two copper plates which can be heated by the surrounding coaxial heaters. Lower temperatures are reached by cooling a copper ribbon, which is attached to the sample holder, using liquid nitrogen. The coolant is located outside the vacuum vessel.

The temperature of the copper plates is monitored by a K-type thermocouple and the electrical heating power is regulated by a PID controller.

To avoid the charging of the glass front plane of the capillary by the incident ion beam, an aluminium foil is fixed directly in front of the capillary's entrance. This foil is covered by graphite and a hole of approximately 120 μm is pinched in it. The aperture has to be perfectly aligned with the sample. Therefore a thin wire of approximately 120 μm diameter is run through the capillary and eventually pins a hole into the aluminium foil. Furthermore the outside surface of the whole capillary is covered by graphite to guarantee symmetry and uniform charge transport and temperature distribution (figure 2.7).

Directly below the capillary entrance there is a reference aperture of 100 μm diameter. By moving the sample holder 25 mm upwards, the reference aperture can be brought into the beam axis. The aperture can give a reference for the incident ion beam intensity and is necessary for 'finding' the capillary's entrance.

In order to ensure that tilting the sample holder does not influence the aperture's lateral

2 Experimental setup

position, both, the capillary entrance and the reference aperture are positioned along the manipulator rod's rotation axis.

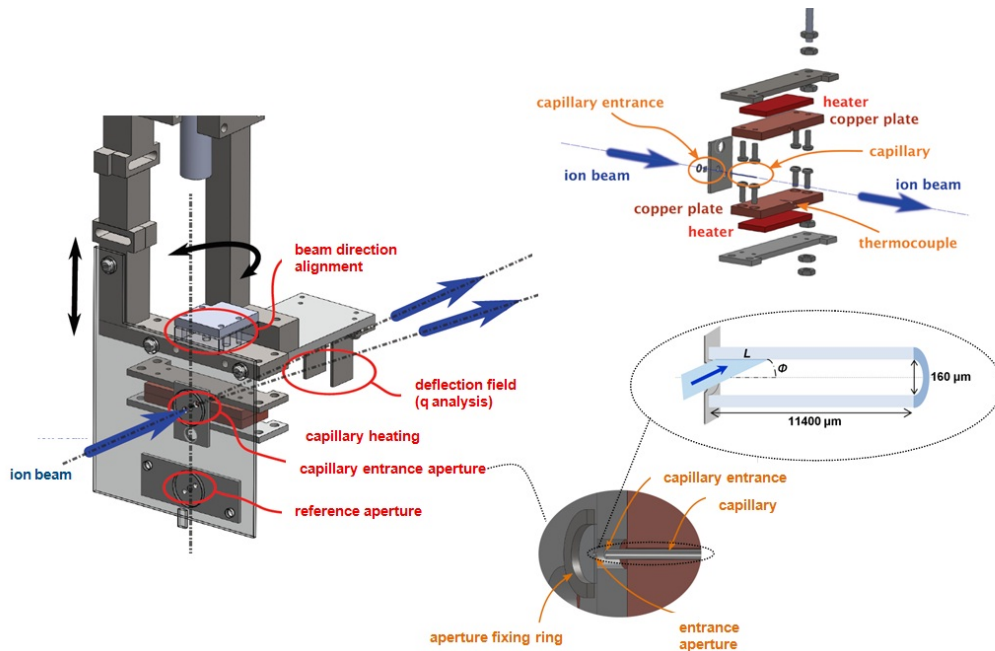


Figure 2.7: **Experimental setup for the straight glass capillary**

The setup enables a temperature variation of the capillary between -35°C and $+90^{\circ}\text{C}$. The incident ion beam hits the capillary entrance aperture or the reference aperture, depending on the z-position of the manipulator, and the transmitted ions are detected by the position sensitive micro-channel-plate detector, located approximately 18 cm behind the capillary entrance. The reference aperture has a diameter of $100\ \mu\text{m}$ and is used for diagnostic and monitoring purposes.

To avoid the charging of the front plate of the glass capillary, an aluminium foil with a pinhole is fixed directly in front of the capillary entrance.

2.5.2 Sample holder for the tapered capillary

For the measurements with the tapered capillary a new sample holder is designed and constructed during the elaboration of this master thesis and described in more detail in [104]. Its major components are a capillary holder, that can be heated, and two reference apertures of 800 μm and 100 μm in diameter.

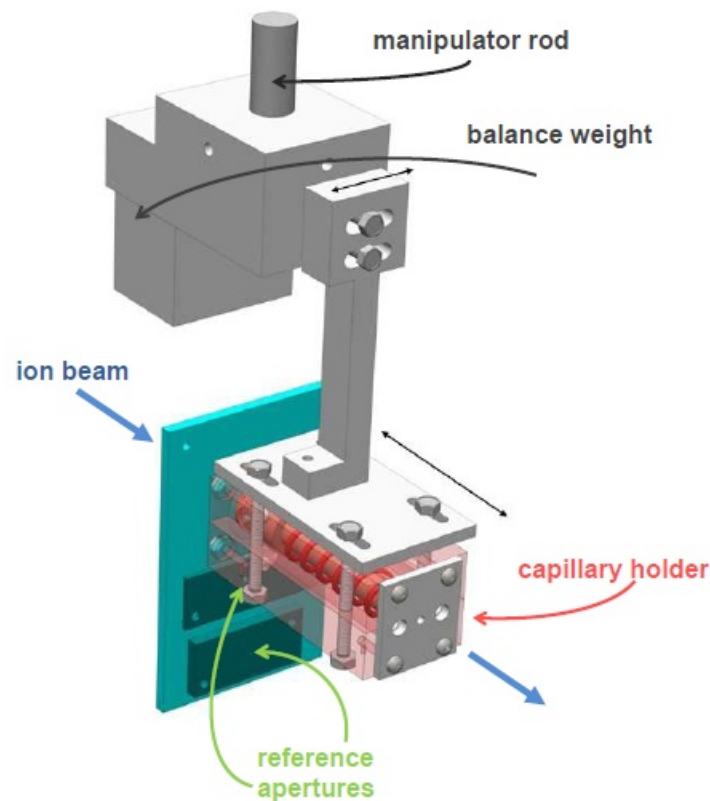


Figure 2.8: **Sample holder for the tapered capillary**

The sample holder is mounted on a manipulator rod which can be moved in x, y, z direction and tilted by ϕ . The capillary entrance and the two reference apertures have to match with the manipulator rod's axis for ensuring that a tilting of the sample does not shift the lateral position of the apertures. The capillary holder can be adjusted horizontally, back- and forwards relative to the rod axis (indicated by the arrows).

2 Experimental setup

The sample holder is mounted on the manipulator rod as seen in figure 2.8. To ensure that the tilting of the sample holder does not shift the lateral position of the capillary entrance and that of the reference apertures, they all have to match with the manipulator rod's rotation axis. For this purpose the capillary holder can be adjusted horizontally, back- and forwards relative to the rod axis.

The sample holder is mounted on the manipulator rod with great care; the assembling was monitored with a camera, enabling a magnification of the individual components and therefore improved positioning.

The reference apertures are located directly below the capillary entrance in a fixed distance (figure 2.9). After guiding the ion beam through the reference apertures, the sample holder is shifted in z -direction and the ion beam is brought into the capillary's axis. Again the reference apertures serve diagnostic and monitoring purposes.

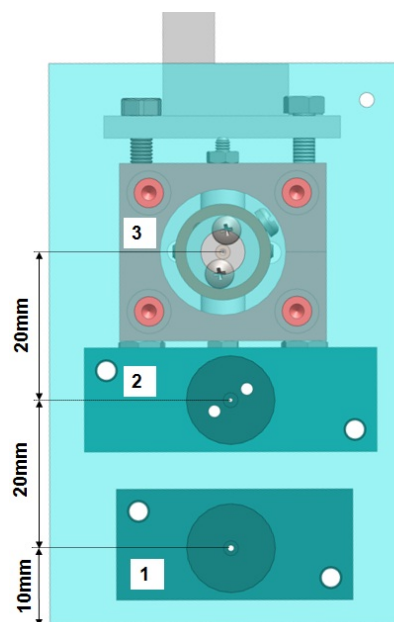


Figure 2.9: **Front view of the sample holder**

- 1) reference aperture: $\varnothing=800 \mu\text{m}$
- 2) reference aperture: $\varnothing=100 \mu\text{m}$
- 3) capillary entrance: $\varnothing=800 \mu\text{m}$

2 Experimental setup

The capillary holder houses the single tapered insulating capillary. It is made of borosilicate glass and has the following macroscopic dimensions (figure 2.10): The outer entrance diameter is 1.5 mm and the inner 0.86 mm. The exit diameter amounts to 82 μm . The 5 mm straight section is followed by a 5 cm long conical part.

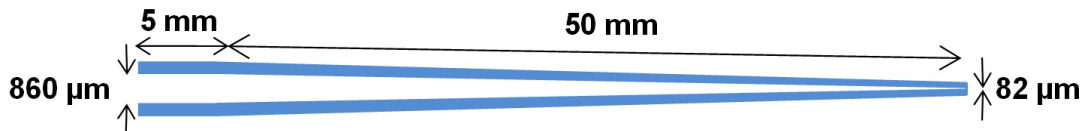


Figure 2.10: Geometry of the tapered capillary with macroscopic dimensions

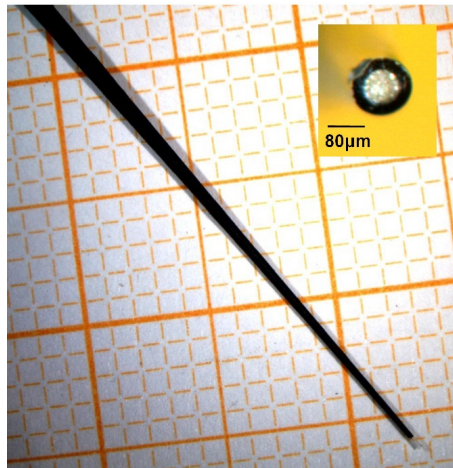


Figure 2.11: Pictures of the tapered capillary

The figure shows the tapered capillary lying on a millimeter paper, the figure in the upper right corner the tip of the capillary.

The straight section of the capillary is placed into a specially designed copper-barrel and tightened with four screws. The conical part of the capillary is surrounded by a hollow copper-barrel, which is screwed into the above mentioned other copper-barrel. The straight adjustment of the capillary is one of the most important and difficult steps during the assembling of the sample holder and is carried out using a reflected-light microscope and checked by a transmitted-light microscope.

Figure 2.11 shows the tapered capillary with a reference length scale. The image in the

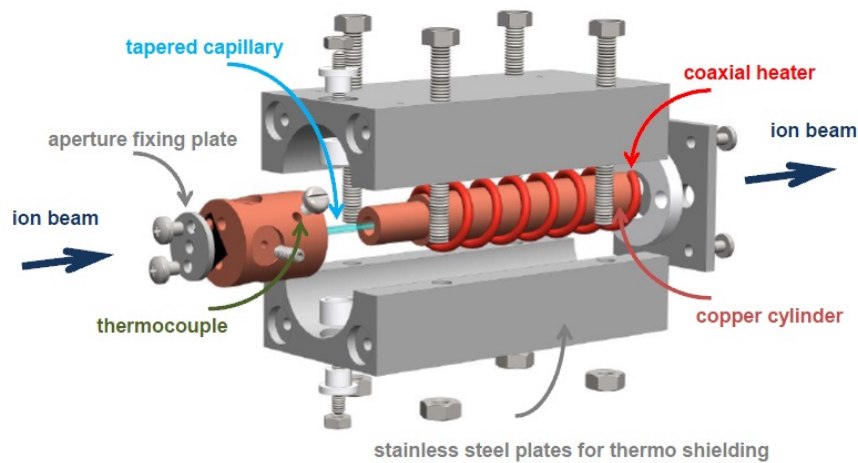


Figure 2.12: **Model of the tapered capillary holder**

The tapered capillary is placed into a specially designed copper barrel, which is surrounded by a coaxial heater and thermo shielded by stainless steel plates (for details see text).

The experimental setup enables a temperature variation of the glass capillary between room temperature and $+90^{\circ}\text{C}$.

upper right corner shows the tip of the capillary. The photo is taken with a reflected-light microscope.

To avoid charging the glass front of the capillary's entrance by the incident ion beam, causing a deflection of succeeding ions, an aperture is used right in front of the entrance. To this purpose an aluminium foil covered with graphite, is fixed in front of the sample and a hole of approximately $800\ \mu\text{m}$ is pinched by a wire into the foil.

To guarantee a uniform charge transport and temperature distribution along the whole capillary, its outside surface is covered by graphite.

The copper-barrel is surrounded by a coaxial heater, which heats the copper part of the sample holder and in succession the glass capillary by thermal radiation. To avoid heat loss to the surrounding, the copper cylinder is thermo shielded by two stainless steel plates surrounding the copper cylinder without contact.

2 Experimental setup

The temperature is monitored by a K-type thermocouple and the heating power is regulated by a PID controller. The experimental setup enables a controlled and uniform temperature variation of the glass capillary between room temperature and $+90^{\circ}\text{C}$.

During the design phase of the tapered capillary holder, some temperature simulations with the software SolidWorks 2009 were performed. The results of these simulations are plotted in the figures 2.13 and 2.14. While figure 2.13 shows the temperature distribution along the glass capillary after the steady state is achieved, figure 2.14 shows the temporal process of the heating of the glass capillary. The four pictures show the temperature distribution along the capillary at four different points of time. Under the initial condition of a 100°C heated copper barrel, the capillary achieves an almost uniform temperature distribution within a short period of time (~ 10 min).

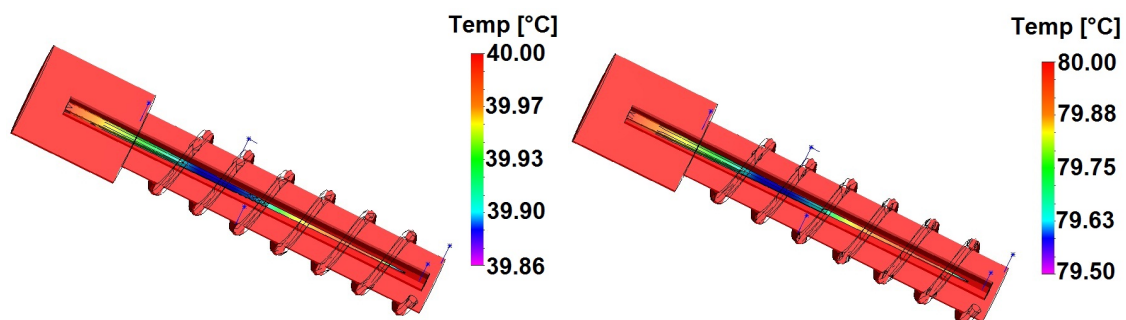


Figure 2.13: **Temperature distribution along the capillary after the steady state is achieved**

In the left figure the temperature of the heater is set to 40°C and in the right figure to 80°C .

The temperature varies only several tenths of a degree along the capillary.

Besides the temperature simulation, some basic calculations (assuming that heat is transmitted only by heat radiation) are performed. The left plot of figure 2.15 compares the results achieved by the calculation with the simulation.

For the simulations some parameters had to be estimated. To check how well the simulation fits the ‘real’ conditions, a simple experiment is conducted. Therefore a K-type

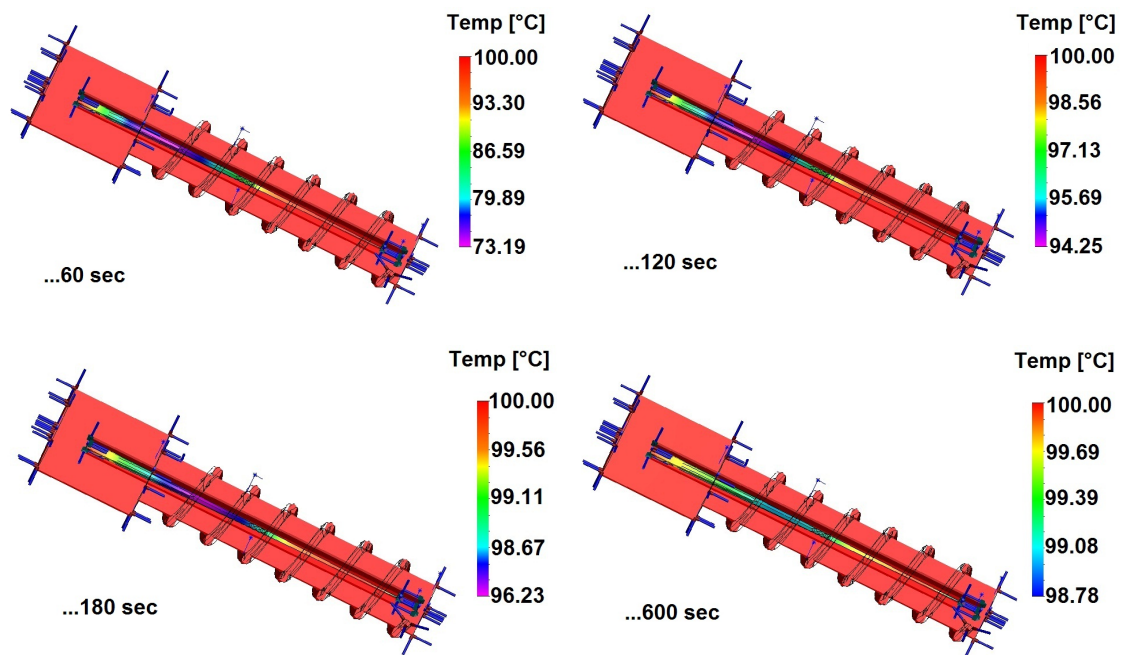


Figure 2.14: **Temperature distribution along the capillary during the heating process**

The coaxial heater is set to 100°C and the figures show the temperature distribution at four different points of time.

thermocouple is stuck on the capillary outer surface (for the measurements another capillary of the same macroscopic dimensions is used) and a second one was fixed on the copper-barrel. The sample holder is mounted on a manipulator and inserted into a standard DN63CF double T-piece. The vacuum vessel is evacuated by a turbo molecular pump and the pressure measured by a Bayard-Alpert pressure gauge. The temperature measurements are carried out at a pressure condition of $\sim 3 \cdot 10^{-8}$ mbar. The temperature values are measured and controlled by a PID controller and the right picture of figure 2.15 shows the temporal process of the heating. The temperature of the copper-barrel represents well the temperature of the capillary.

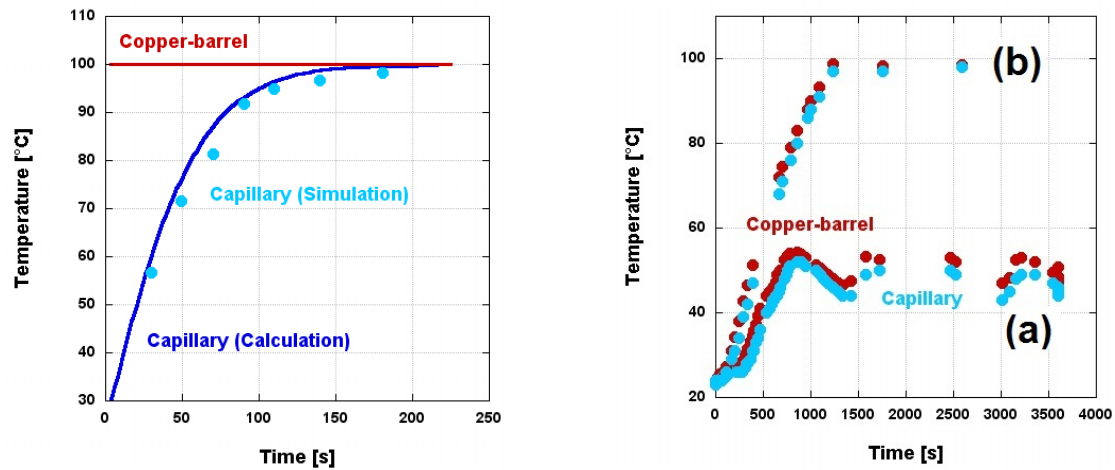


Figure 2.15: **Testing the heating of the glass capillary**

left: The solid line shows the calculated (for the calculation the heat is transmitted only by heat radiation) temporal process of the heating of the capillary in the case that the copper-barrel has a temperature of 100°C. The points are the results of a simulation carried out with the Software programme SolidWorks2009.

right: Temporal process of the heating of the sample holder; One pair of curves shows the slow increase of the heating current ((a) 23°C→~ 50°C in ~ 15 min) and the other one the heating process without heating breaks((b) 23°C→~ 100°C in ~ 15 min). The temperature of the copper-barrel (red lines) represents quite well the temperature of the glass capillary (blue lines). The heating current is regulated by a PID controller.

2.6 Measuring procedure

Before starting any series of measurements, proper source-operating-parameters for the production of a stable ion beam at a certain charge state and a certain kinetic energy have to be found. Because of the fact, that until now there is no primary beam monitor right next to the capillary entrance, which allows to judge on the stability of the incident ion beam, it is tried to check the stability by measuring the current on the first two apertures of the beamline. Usually, at the first aperture a current of a few nanoamperes is measured and at the second aperture a current of a few tenths of picoamperes. It is tried to achieve almost stable ion beam conditions with fluctuations of only a few picoamperes on the second aperture.

If the incident ion beam seems to be stable enough, the beam is guided by the beamline's electrostatic lens system into the experimental chamber. For determining the proper voltages of the deflection plates of the lens system, it is advisable to begin with high incident ion intensities. In this case the ion current is great enough to be measured at the sequenced apertures and the ion beam can be guided from one aperture to the next, until it hits the last lens element. During this prearrangement period no voltage is applied at the detector to prevent any damage. After measuring the current on the last lens element, the incident ion intensity has to be reduced and the detector can be 'switched on'. The sample holder is totally moved out of the beam's pathway and the whole ion beam can be monitored on the PSD by adjusting the deflection plates directly in front of the last lens element.

Afterwards the ion beam has to be brought to the capillary's entrance. Therefore the reference aperture(s) of the sample holder is/are used. The sample holder is moved slowly into the beam's pathway until only half of the primary count rate is detected. At this point it can be suggested that the ion beam hits the lower frame of the sample holder. Moving then the sample holder 10 mm downwards, should bring the ion beam into the

right z-position. Thereupon, the sample holder is moved horizontally, until the beam can be detected on the PSD. In order to facilitate this process, the aperture's centre position can be determined optically with a camera, which is mounted on the outside of the vacuum chamber.

In the next step, the sample holder is moved upwards for 25 mm (in the case of the straight capillary) or rather for 10 mm (in the case of the tapered capillary) and the ion beam hits the capillary entrance and is eventually guided through it.

In steps of usually less than 1° the capillary is tilted into one direction and the data is stored until the transmission vanishes. Then the capillary is tilted into the opposite direction and the measurements are repeated as described before until the transmission vanishes again.

For diagnostic and monitoring purpose, it is advisable to detect the amount of transmitted ions through the reference apertures before and after each series of measurements.

For each collection of data the forward direction has to be determined anew, because the capillary's straight direction is always defined with respect to the incoming ion beam direction.

For the straight capillary the transmission curves can be fitted by a Gaussian function and eventually shifted along the tilt angle axis to provide a tilt angle axis centered at the direction of maximum transmission.

For the tapered capillary the transmission curve can no more be described by a simple Gaussian fit, but by a more sophisticated function with a distinct drop towards the forward direction has to be used. Also in this case the datapoints are slightly shifted afterwards along the tilt angle axis to provide that the local minimum coincide with the straight direction.

Due to the fact that the capillary can be tilted only in one plane, the straight direction can be found by increasing the temperature of the capillary. Increasing the temperature leads to an increasing of the electrical conductivity, which results eventually in the vanishing of the guiding effect and therefore in the coincidence of the transmission curve with the geometric limited transmission through the capillary.

At higher temperatures the transmitted ion intensity can be optimized by adjusting the voltages applied to the deflection plates. Afterwards the capillary is cooled down and further measurements can be performed without changing any parameters or voltages. This procedure is recommended for measurements with the straight capillary and necessary for measurements with the tapered capillary.

In contrast to the straight capillary, the sample holder for the tapered capillary enables the heating/cooling only by heat radiation. Therefore the cooling process of the capillary takes several hours. During this period and the following measurement time the incident ion beam intensity has to remain stable. This is one of the crucial points of the measurement procedure.

The high stability of the incident ion beam over a longer period of time (several hours) is also necessary for the measurements with the straight capillary at lower temperatures to monitor the movement of the transmitted particles on the PSD. Also in this case, the challenge is to find the right parameters to keep the incoming ion beam stable.

3 Results

3.1 Straight capillary

3.1.1 Ion transmission as function of different temperatures and incident ion fluxes

The first measurements with the single straight macroscopic glass capillary, performed by Kowarik et al. [82], show that the tuning of the electrical conductivity of the capillary with temperature (see figure 3.1) and the intensity of the incident ion flux are two important key parameters for ion transmission control. To verify and expand these preliminary results, further measurements are performed during the elaboration of this thesis and will be presented now in more detail.

The new measurements are performed with Ar^{q+} -ions at a kinetic energy of 4.5 keV and a charge state of $q=7$ instead of the $q=9$ as in the experiments of Kowarik et al. [82]. Although the capillary guiding effect appears more powerful for ions in higher charge states, the use of Ar-ions at lower charge state is favored because of the higher stability of the extracted ion beam. Consequently longer measurement periods are possible. A further modification in comparison to the previous measurements is the exchange of the wedge-and strip anode. The old wedge-and strip anode already showed some areas with very low efficiency and is therefore of limited use for measurements as described in section 3.1.2. Unfortunately, the efficiency of this new anode is not perfectly homogeneous either.

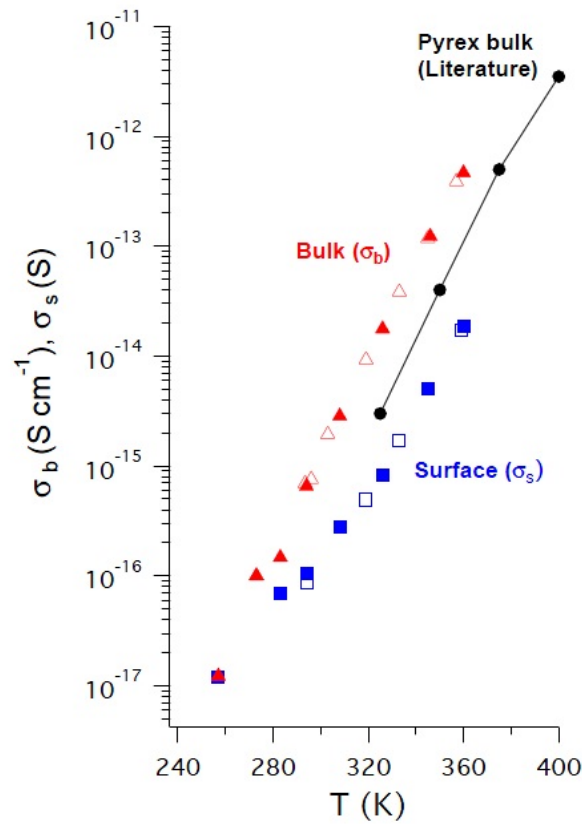


Figure 3.1: **Temperature dependence of the electrical conductivity** [105]

As a first step, the intensity of the ion beam, transmitted through the capillary, is measured as a function of the tilt angle ϕ . The straight position of $\phi=0^\circ$ (=no tilting angle between incident ion beam and capillary) is determined by geometrically maximizing the transmitted intensity. Afterwards the capillary is stepwise tilted, first in one direction and afterwards in the other, until transmission is negligible.

After a charging time of some hundred of seconds, an equilibrium between deposited charges and transmitted ions is reached and the transmission intensity saturates. This saturation value is dead-time corrected and shown as one data point in the transmission curve for each tilt angle. The points are fitted by a Gaussian, which is then normalized with respect to the transmission in forward direction. After fitting, the centre position is determined and the data points are shifted for each individual curve.

Figure 3.2 and 3.3 show such transmission curves for different capillary temperatures. The flux of the incident ions is kept constant at about 5 keps on the PSD in $\phi=0^\circ$ direction for the data points shown in figure 3.2 and at about 2 keps for the data in figure 3.3.

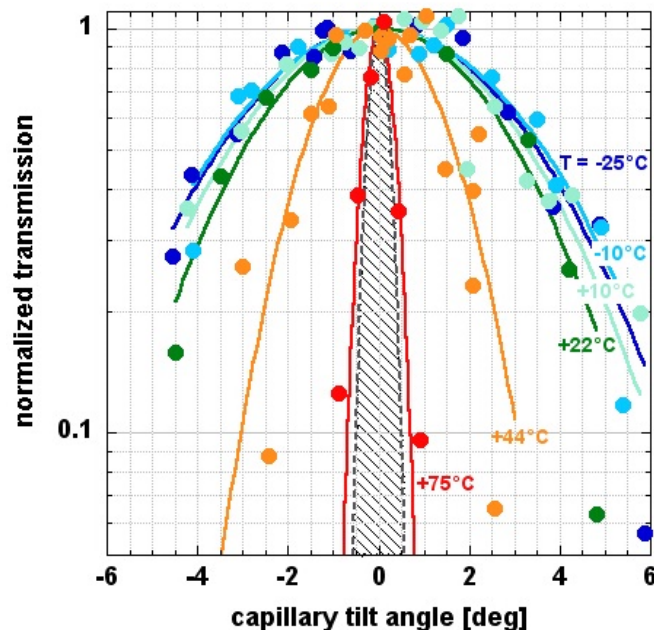


Figure 3.2: **Transmission curves at different temperatures and a constant incident ion flux of 5 keps**

Normalized transmission curves for 4.5 keV Ar^{7+} ions guided through a straight glass capillary. Gaussian fits through the data points are shown as solid lines. The capillary's temperature T is written as parameter. The geometric transmission region is shown as hatched area. The monitored count rate on the PSD is around 5 keps for all of the plotted curves in forward direction.

The temperature-dependent guiding angle ϕ_c is determined by the $1/e$ drop of the intensity

$$I(\phi_c, T) = I(0, T)e^{-\frac{\phi^2}{\phi_c^2}} \quad (3.1)$$

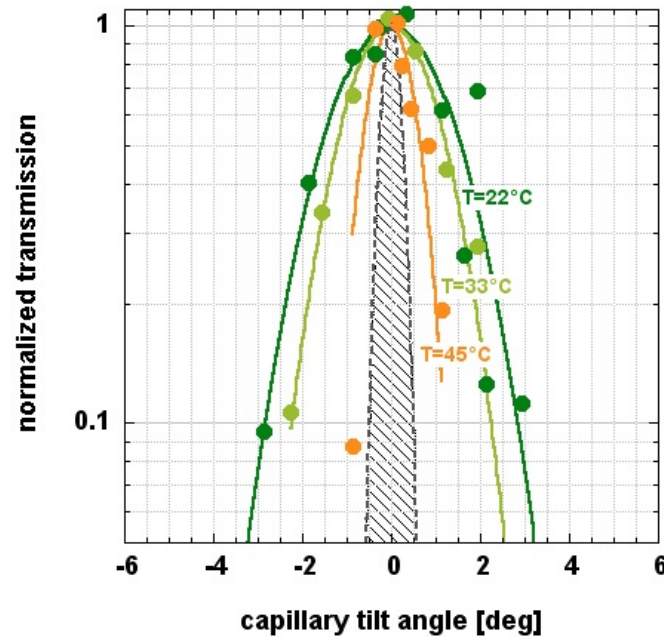


Figure 3.3: **Transmission curves at different temperatures and a constant incident ion flux of 2 kcps**

Normalized transmission curves for 4.5 keV Ar^{7+} ions guided through a straight glass capillary. The monitored count rate on the PSD is around 2 kcps.

Near room temperature stable guiding condition with a guiding angle of $\phi_c=3.5^\circ$ can be observed. In agreement with the earlier measurements, the increasing of the capillary's temperature, hence conductivity, leads to a considerable narrowing of the transmission curve and decreasing of the respective guiding angle. Above 75°C the transmission curve approaches a temperature-independent transmission function, which corresponds to the geometric transmission through the capillary. For the used macroscopic capillary (length: 11.4 mm, inner diameter: $160\ \mu\text{m}$) the geometric transmission region relates to $\pm 0.8^\circ$ and is marked in figure 3.2 and 3.3 as hatched area.

At these temperatures the conductivity of the glass capillary is high enough that the charge patches are quickly removed and consequently guiding conditions are prevented.

Below room temperature the transmission curves become slightly larger, however additional dynamic instabilities of the transmitted ion beam spot on the PSD can now be observed (see section 3.1.2).

Besides the influence of the electrical conductivity on the guiding process, also the incident ion flux as parameter for transmission is investigated in more detail. Figure 3.4 shows the transmission curves for various incident ion flux values at room temperature. The increasing of the incident ion flux leads to an increased guiding angle.

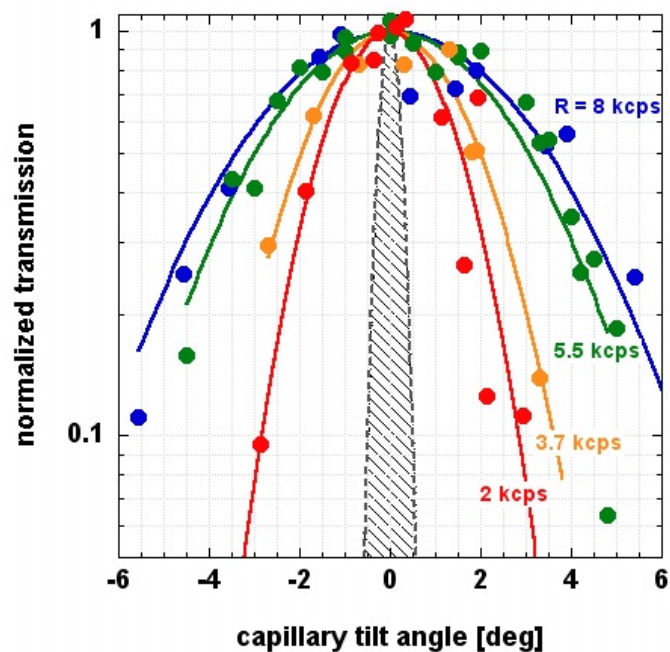


Figure 3.4: **Transmission curve at room temperature for different incident ion fluxes**

Normalized transmission curves for 4.5 keV Ar^{7+} ions guided through a straight glass capillary at room temperature. Gaussian fits through the data points are shown as solid lines. The transmission intensity in cps in straight direction $\phi=0^\circ$ is written as parameter. The geometric transmission region is shown as hatched area.

3 Results

Thus, the guiding power, measurable by the guiding angle, depends on the one hand on the conductivity and on the other on the incident ion flux. Increasing the temperature at constant incident ion flux or decreasing the ion flux at constant temperature leads to a decreasing of the guiding angle and vice versa.

Extracting the guiding angle from the fitted transmission curves and plotting them versus the temperature or rather the count rate in forward direction, summarizes the described results and makes the trend easily visible (figure 3.5).

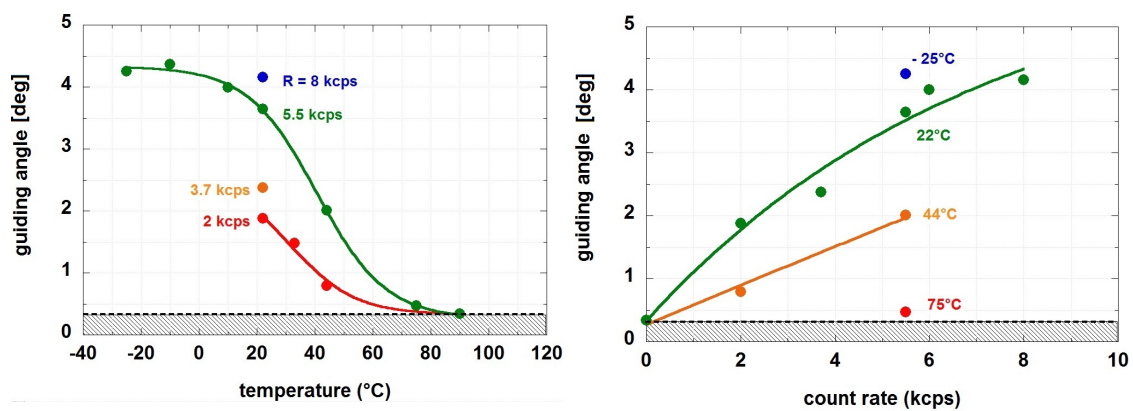


Figure 3.5: **Variation of the guiding angle with temperature and incident ion flux**

left: Measured guiding angle as a function of capillary temperature for various projectile count rates.

The solid lines fit the data points. At high temperatures the guiding angle approaches with the geometric limited angle while at low temperatures the guiding angle saturates.

right: Measured guiding angle as a function of ion count rate for various capillary temperatures.

The fitted solid lines through the data points show the direct relationship between guiding angle and incident ion intensity.

The count rate is the measured transmission intensity in forward direction.

The hatched area represents the geometric transmission region.

Besides the increase/decrease of the guiding angle in dependency of the temperature and the incident ion flux, a rather different behaviour of the transmitted ion beam for different capillary tilt angles is observed. While for tilting angles close to the forward direction the transmitted ion intensity is quite stable (observed instabilities can be explained by an unstable incident ion beam), the count rate fluctuates considerably for larger tilt angles. An example is shown in figure 3.8.

The measurements however confirm the previously found linear relation between the deflection and tilting angle (figure 3.6). To determine the deflection angle, the beam spot position on the PSD is used. 2D images of the beam spots for 5 different capillary tilt angles are plotted in figure 3.7. The data points represent the summarised count rate over the same measurement period of time.

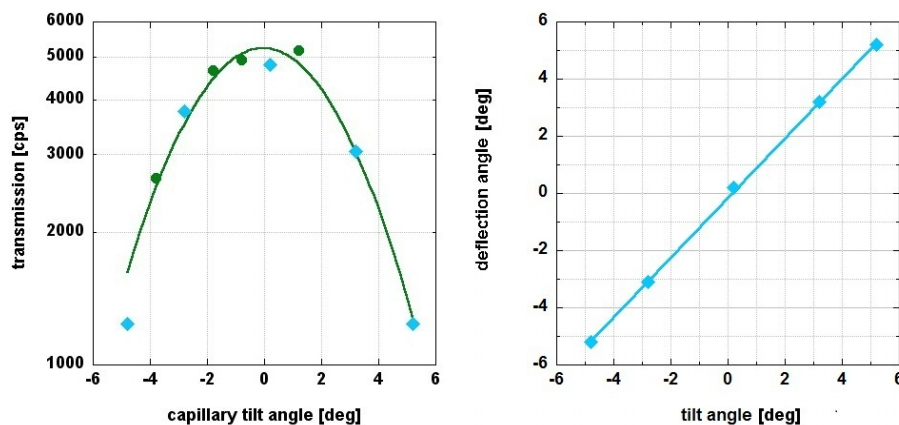


Figure 3.6: **Linear relation between tilting and deflection angle**

left: The figure shows again the transmission curve at room temperature. The solid line represents the Gaussian through the data points. For the five blue colored rhombic data points 2D images on the PSD are plotted in figure 3.7.
 right: The figure shows a linear relation between the tilting and the deflection angle. The deflection angles are calculated from the beam spot position on the PSD and correspond to the blue colored rhombic intensity points in the left figure.

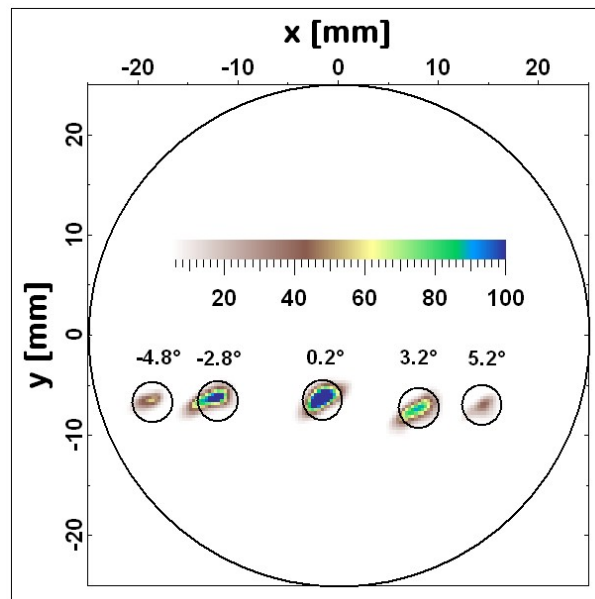


Figure 3.7: **The lateral position of the transmitted ion beam for five different capillary tilt angles**

The intensity distributions are shown for equal measurement durations. The intensity of the transmitted ions is colour coded. Blue corresponds to the maximal transmitted intensity and is set at 100 per cent of the colour scale. The colour distributions of the 2D images have to be read relative to this maximal transmission. The yellow colour for example shows 60 per cent intensity compared to the maximum.

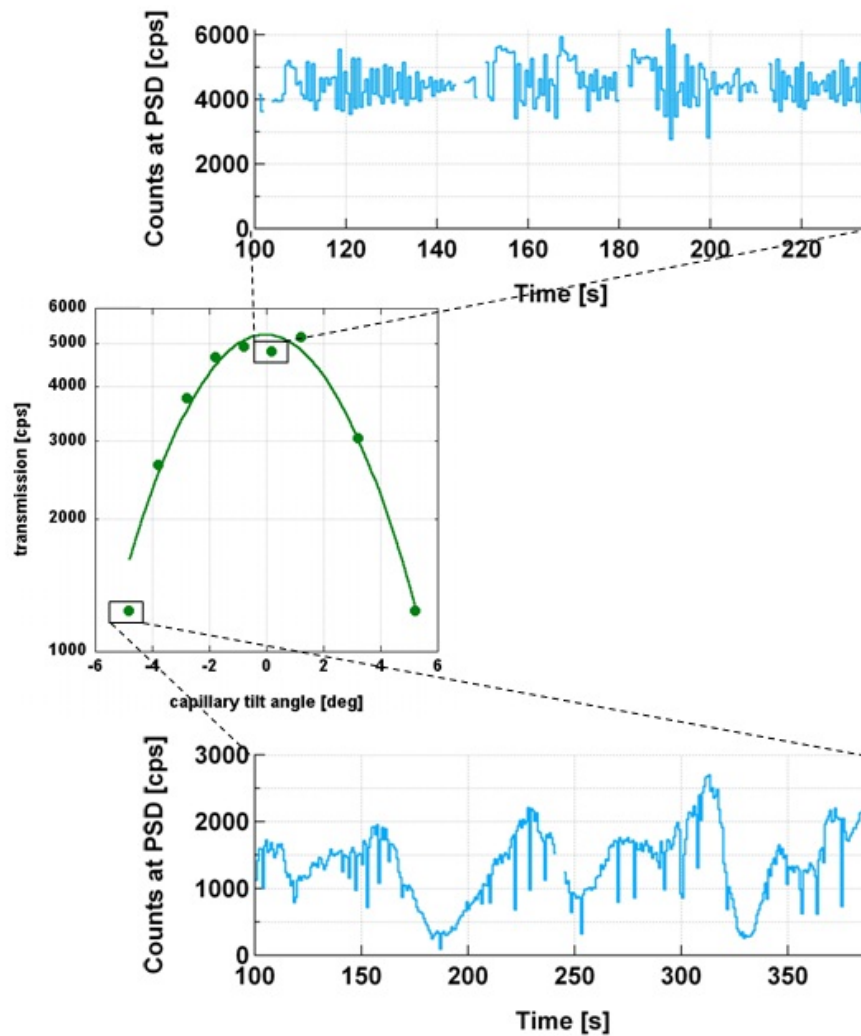


Figure 3.8: **Variation of the transmitted intensity at different tilt angles**

The figure in the middle shows the transmission curve at $T=22^{\circ}\text{C}$. The data points represent the mean value of the dead-time-corrected count rate. For the signed data points the transmitted intensity is plotted versus the elapsed time. While the transmitted intensity seems to be rather stable for the tilting angle of $\phi=0.2^{\circ}$, it considerably oscillates for a large tilting angle of $\phi=4.8^{\circ}$

3.1.2 Temperature dependent movement of the beam spot on the PSD

Besides the slight increase of the guiding angle at very low temperatures (i.e. below room temperature), dynamical instabilities of the transmitted ion beam spot on the PSD can be observed. The beam spot on the PSD becomes time-dependent and performs a random motion.

The beam spot movement at lower temperatures was already been described in [82] and the corresponding measurements have been repeated during this master thesis to check their validity.

Figure 3.9 illustrates the center-of-gravity motion on the PSD during the cooling process of the capillary from $+35^{\circ}\text{C}$ to -25°C . The capillary remained tilted at 2° for the whole measurement and the cooling evolution is color coded.

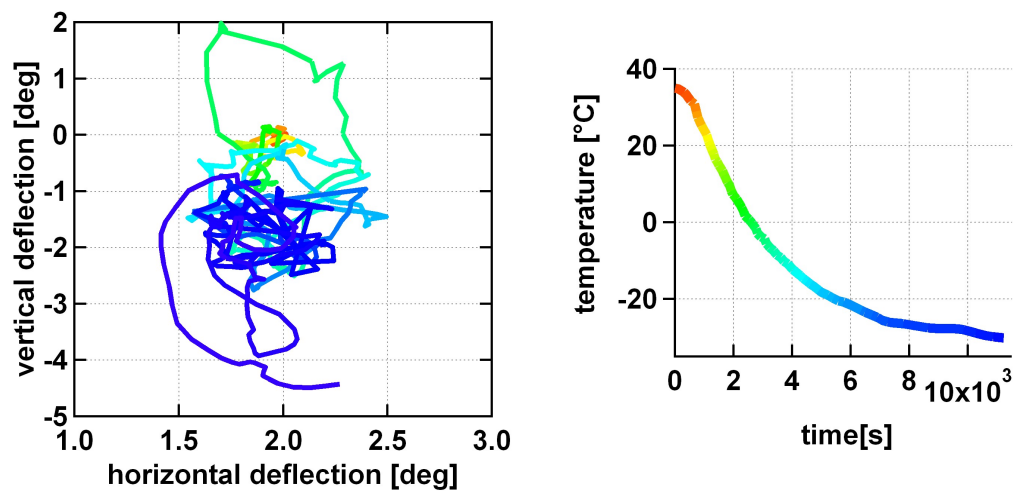


Figure 3.9: **Random motion of the beam spot during the cooling process**

Center-of-gravity motion of Ar^{7+} ions transmitted through the glass capillary on the PSD during the cooling process from $+35^{\circ}\text{C}$ to -25°C . The capillary was tilted 2° before starting the measurement. The temperature is colour coded. The right figure shows the exponential decreasing of the capillary temperature during the cooling process and gives the colour code.

3 Results

The angular range, which the beam spot covers by moving on the PSD, increases with decreasing temperature. The wide angular variation suggests strong fluctuations of the charge patches in the capillary. Due to the fact that the angular range of the beam spot exceeds the geometric opening angle by far, the fluctuations of the charge patches are most likely located near the capillary exit.

Due to the fact that during the cooling period the capillary is thermally not in equilibrium, it is possible that charge patch fluctuations resulting from the lower electrical conductivity are superimposed by fluctuations caused by temperature variations.

To prevent such additional fluctuations, the movement of the transmitted beam spot is recorded again at different temperatures, but this time the capillary is kept at a certain temperature for a longer time (>10 min) before bringing the capillary into the ion beam and recording the movement of the transmitted ion beam on the PSD. The results of this measurement are plotted in figure 3.10.

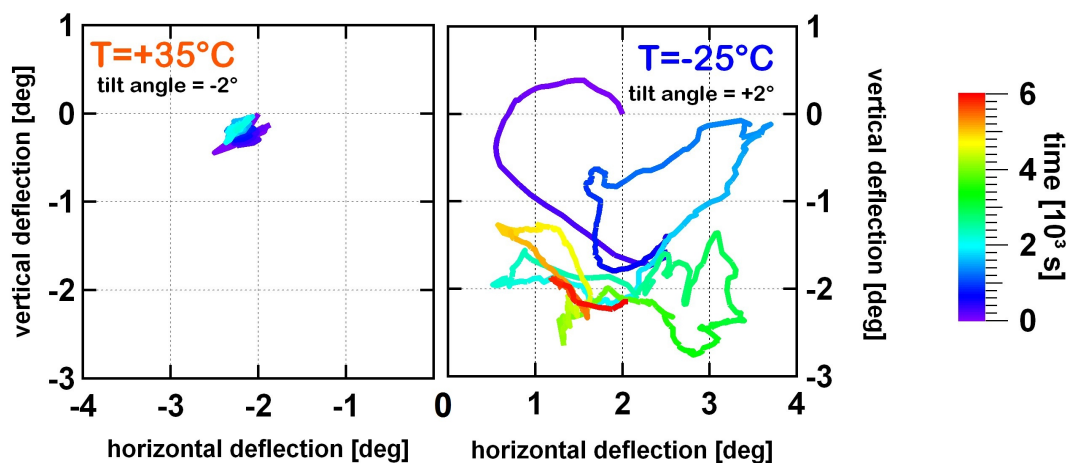


Figure 3.10: Comparison of the motion of the transmitted beam spot at two different temperatures

Center-of-gravity motion of Ar^{7+} beam transmitted through a glass capillary, tilted by 2° . The elapsed time is indicated by colours.

In this case the random motion can be observed at low temperatures in contrast to the heated capillary, where the beam spot position is stable for hours, showing only small spatial fluctuations associated to the time evolution of charge patches inside the capillary. This results again confirm the measurements presented in [82].

Furthermore, it is investigated how much the charging history of the capillary influences the transmission at lower temperatures. Therefore, an additional measurement at -25°C is performed, but this time the ion beam is kept turned on during the cooling process. Recent measurements [82] had indicated that under such conditions stable transmission at temperatures as low as -30°C are possible without major movements of the beam spot (figure 3.11). This was explained by freezing the existing charge-patches and so keeping up stable transmission even at very low conductivity.

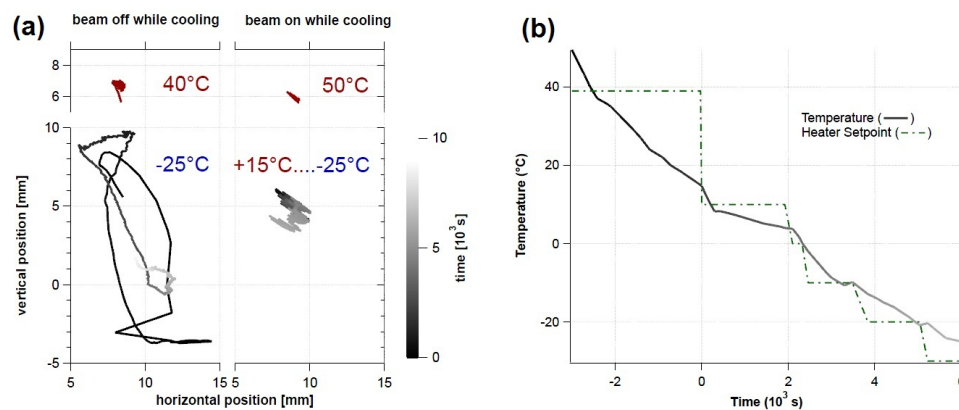


Figure 3.11: **Comparison between beam on/off while cooling, taken from [82]**

(a) The beam spot movement is illustrated as a function of time (colour coded). The upper part of the figure shows the position of the transmitted ion beam on the detector for the heated capillary case. The left part shows the movement at lower temperatures for the case that the ion beam is turned off during the cooling process and is in strong contrast to the right part of the figure, where the beam is kept turned on during the cooling process. The temperature evolution for the smooth cooling case is shown in (b).

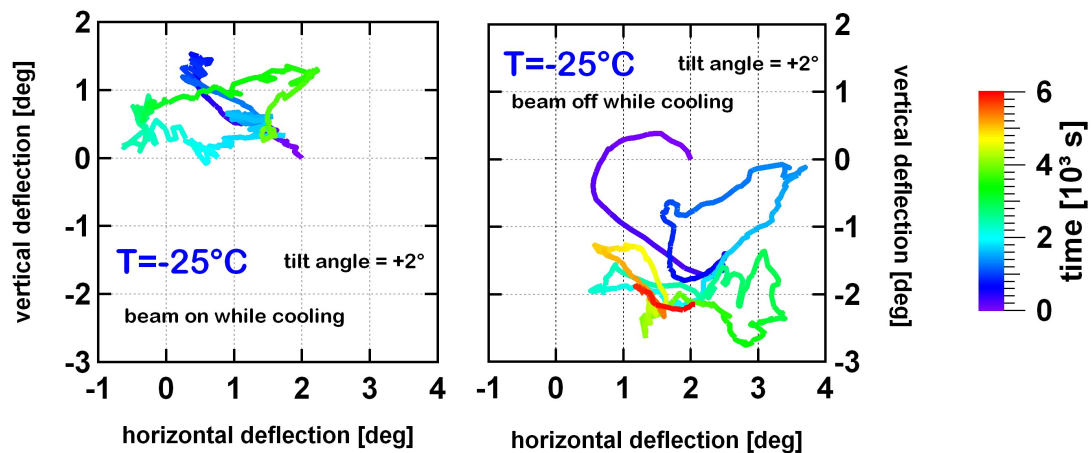


Figure 3.12: Comparison of the motion of the transmitted beam spot for two different cooling processes

The lines show the center-of-gravity motion of the transmitted beam spot on the PSD. In the left figure the incoming ion beam is turned on during the cooling process and in the right figure the beam is turned off. Both measurements are started as soon as the capillary is in a thermal equilibrium at $T=-25^{\circ}\text{C}$. In both cases Ar^{7+} -ions at a kinetic energy of 4.5 keV are used and the capillary is tilted by 2° .

Newer measurements however, can not reproduce this observation. The situation is illustrated in figure 3.12, where the right figure shows the situation, where the temperature is first set to -25°C before switching the ion beam on. The left figure shows the situation, in which the ion beam stays switched on during the cooling of the capillary. Before these measurements are performed, the capillary is aligned at an elevated temperature ($+35^{\circ}\text{C}$) with respect to the incident ion beam.

It seems indeed that the movement of the beam spot covers a smaller angular range on the PSD for the ‘beam-on-while-cooling’ case compared to the ‘beam-off-while-cooling’ case, but, nevertheless, the newer measurements strongly differ from the illustrated observation in figure 3.11.

Since the graph in figure 3.11 was obtained in a single, non-repeated measurement, it is

hard to determine the reason for this discrepancy.

Also the extremely strong variations of the transmitted intensity reported earlier [82] can not be reproduced. The newer measurements support the assumption that variations of the primary ion beam were responsible for the observed fluctuations.

3.2 Tapered capillary

The first measurements with a macroscopic tapered capillary already show the existence of the guiding effect up to tilt angles of several degrees [56]. At room temperature however, at very small tilt angles close to the forward direction, the transmission drops significantly [56, 85, 86]. These authors had studied the transmission of ions through tapered glass capillaries at small capillary tilt angles, low incoming ion beam energy and high beam intensity and tried to explain this phenomenon by the so-called blocking effect. A uniformly charged ring-shaped region in the tapered part of the capillary could be responsible for repulsive Coulomb forces which consequently cause the blocking.

In the following the results of the measurements with the tapered capillary, which are carried out during the course of this master thesis, are presented. It is studied how the change of conductivity influences the guiding power and whether the claimed suppression in forward direction can be confirmed by increasing the temperature of the capillary.

The measurements are performed with Ar^{q+} -ions ($q=7,8$) at a kinetic energy between 4.5 and 16 keV. The temperature of the capillary is varied between room temperature and $+90^\circ\text{C}$.

3.2.1 Guiding effect of tapered capillaries

The first still preliminary measurements with the tapered capillary at room temperature show the predicted drop of the transmission at a capillary tilt angle of 0° . The measured transmission curves can be fitted by a Gaussian ansatz (figure 3.13):

$$f(x) = a \cdot e^{-\frac{x^2}{2 \cdot \phi_{c1}^2}} - b \cdot e^{-\frac{x^2}{2 \cdot \phi_{c2}^2}} \quad (3.2)$$

with $b < a$ and $a, b > 0$

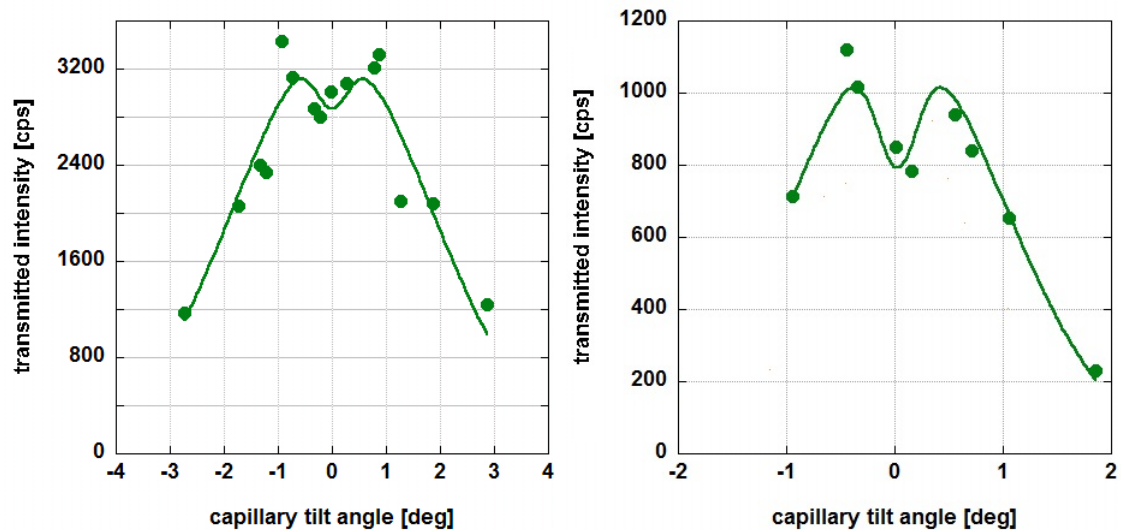


Figure 3.13: **Transmission curve at room temperature**

The two plots show the transmission curve for two different energies (left: 7 keV, right: 4.5 keV) of the incident Ar^{7+} ion beam at room temperature. Both plots show a local minimum of the transmission in forward direction. The solid line represents the fit through the measured data points according to eq. (3.2).

The parameter ϕ_{c1} is the guiding angle of the Gaussian ansatz. The second part of the fit function represents the ‘suppression’ of the transmission at small tilt angles. The power and the width of the suppression are characterised by the parameters b and ϕ_{c2} . As just seen for the straight capillary, after a charging time of several hundred seconds, a

saturation value of the transmission is reached. Figure 3.14 shows such a charging curve. The corresponding transmission curve is plotted in figure 3.15. The data points over the various capillary tilt angles represent the saturation value of each charging curve. From the centre of gravity of the measured distribution on the PSD the beam deflection angle can be extracted. Plotting the deflection angle against the capillary tilting angle, a linear relation is again observed (figure 3.15).

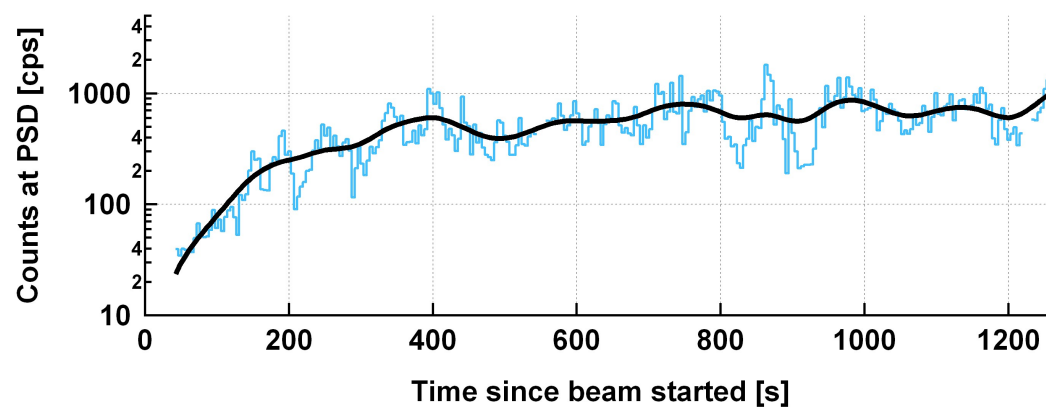


Figure 3.14: **Charging curve of the transmitted ions**

As soon as the beam is turned on, the count rate of the transmitted ions is recorded. The blue line represents the measured count rate over the elapsed time and is smoothed by the black line. After a charging time of approximately 400 sec., a saturation value is reached.

This measurement is performed with 16 keV Ar^{8+} ions at room temperature and the capillary is tilted by 2° .

Although after some hundreds of seconds the transmission value saturates, from time to time rapid fluctuations of the transmitted ion intensity can be observed, particularly in the range of maximum transmission (see figure 3.16). Because of the fact that this oscillation behaviour can be measured several times, it can be traced back to the formation process of the patches instead of fluctuations of the incident ion flux. For taking a closer look at this oscillation, the fast Fourier transform of the count rate is computed. Until

now, no certain periodicity of the appearing eruptions could be recognized.

At higher temperatures the oscillatory behaviour can no longer be detected.

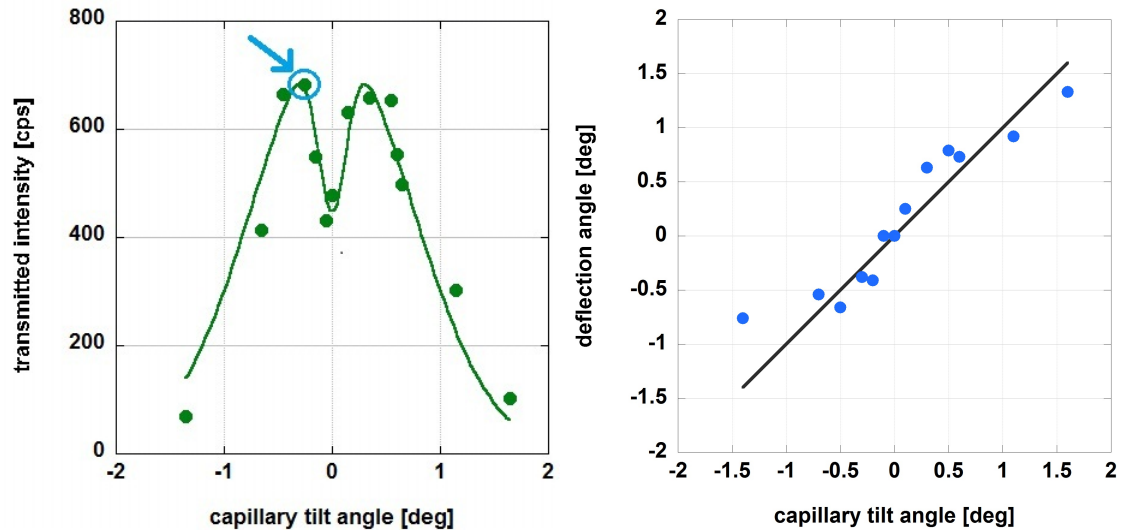


Figure 3.15: **Linear relation between the tilting and deflection angle**

left: The figure shows the transmission curve of Ar^{8+} -ions at a kinetic energy of 16 keV. The transmission curve is monitored at room temperature and shows a suppression of the transmitted ions in forward direction. For the highlighted data point the charging curve is plotted in figure 3.14. The solid line shows the fit through the data points according to eq. (3.2)

right: The figure shows the almost linear relation between the tilting and the deflection angle, which was previously observed for the straight capillary and is well known from the literature. The deflection angle is thereby reconstructed by the measured peak position of the transmitted ion beam on the PSD.

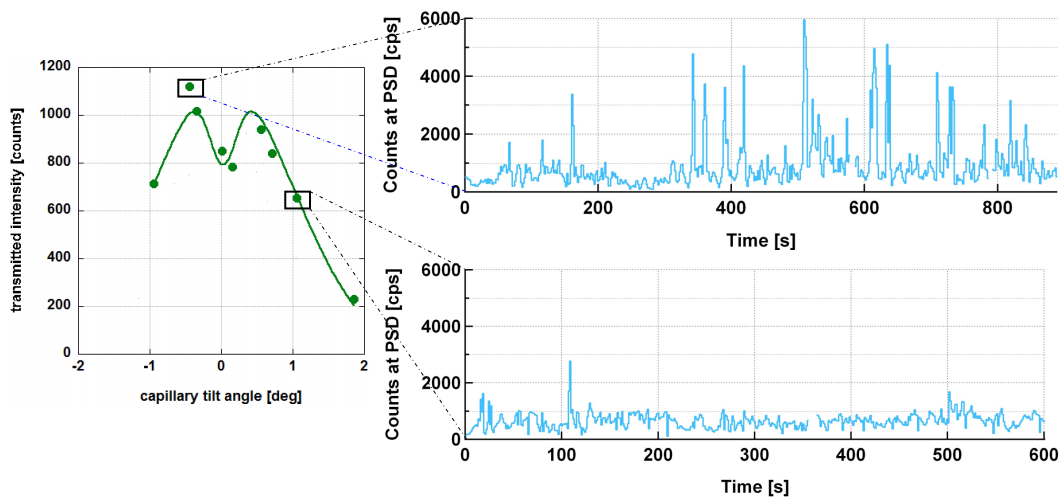


Figure 3.16: **Rapid fluctuations of the transmitted ion intensity**

From time to time rapid fluctuations of the transmitted ion intensity can be observed, especially in the range of maximum transmission. At higher temperatures the fluctuations can no longer be observed.

3.2.2 Ion transmission for different temperatures

After the first measurements, which showed the expected transmission behaviour, further investigation of transmission curves at different temperatures are conducted. As just seen for the straight capillary, increasing temperature (=increase of the electrical conductivity) causes decreasing guiding power. Besides this known effect, it seems that heating the capillary terminates the transmission suppression in forward direction.

Figure 3.17 shows the data points for the measured transmission curve at two different temperatures.

The geometric transmission region is again shown as a hatched area and correlates with the transmission curve at high temperatures.

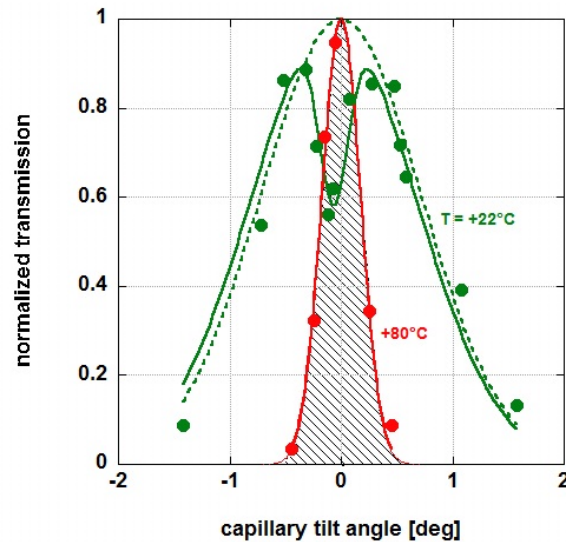


Figure 3.17: **Normalized transmission curves at different temperatures**

Normalized transmission curves for 16 keV Ar^{8+} ions through the tapered capillary at two different temperatures (green: 22°C, red: 80°C). The transmission at 80°C is fitted by a Gaussian which correlates with the geometric transmission region (hatched area). The transmission curve at room temperature is fitted by equation (3.2)

In order to get more information about the transmission at different temperatures a whole series of measurements are performed using Ar^{7+} ions as projectiles; after finding the right ion source parameters for a stable incident Ar^{7+} ion beam, several transmission curves at various temperatures are recorded. The incident ion flux is kept constant during the heating and cooling period. Figure 3.18 shows the result of such a measurement series, one with Ar^{7+} at a kinetic energy of 4.5 keV and the other with Ar^{7+} -ions at a kinetic energy of 7 keV. This time the transmission curves are not normalized but represent the measured count rate at the PSD.

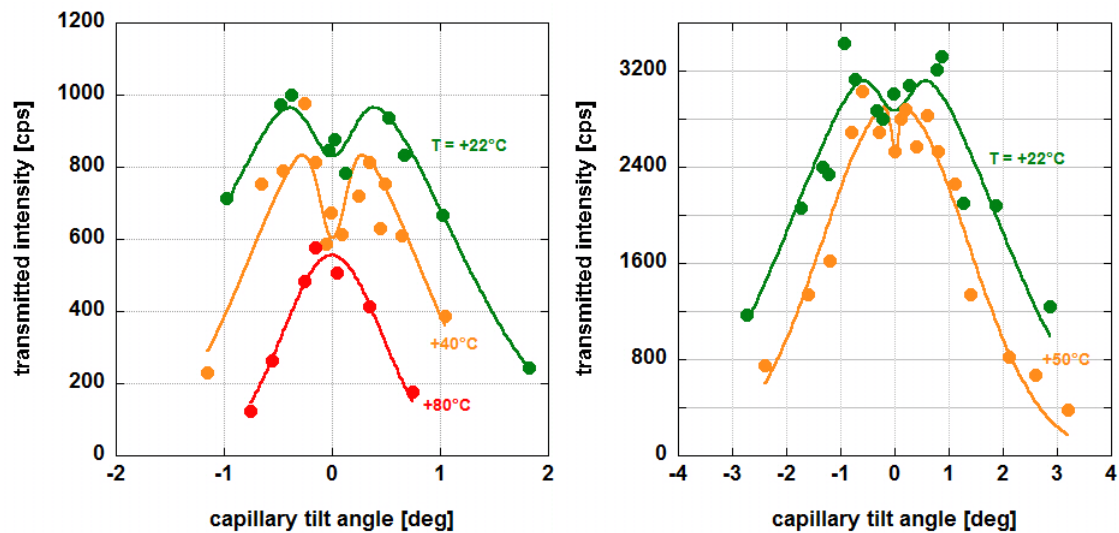


Figure 3.18: **Transmission curves at different temperatures**

The two figures show the results of a series of measurements. The incident ion beam current is kept almost constant during the cooling and heating process and the whole measurement period. The data points represent the measured and dead-time corrected count rate on the PSD. The measurements indicate that besides the decreasing of the guiding power with increased temperature also the transmitted intensity is reduced.

left: transmission curve of Ar^{7+} -ions at a kinetic energy of 4.5 keV at three different temperatures (green: 22°C, orange: 40°C, red: 80°C)

right: transmission curve of Ar^{7+} -ions at a kinetic energy of 7 keV at two different temperatures (green: 22°C, orange: 50°C)

Both figures show that with increasing temperature, the transmission profile gets more narrow, while the drop of the transmitted intensity in forward direction decreases and vanishes at high temperatures.

It seems that an increasing temperature causes a decreasing transmitted intensity even in forward direction. Therefore, it is questionable that the ‘suppression’ in forward direction at lower temperatures is really the result of a blocking effect caused by Coulomb forces as claimed in the literature [85]. The higher transmitted intensity at room temperature as

compared to the higher temperature case (90°C) can also be related to a focusing effect due to real guiding, while, however, is more favorable for the slightly asymmetric case (small but non-zero tilt angle).

The following measurement is performed in order to observe the change in intensity of the transmitted ions in forward direction in dependence of the temperature: In the first step the capillary is heated up to 80°C and the voltages at the deflection plates directly in front of the capillary entrance are adjusted for maximizing the transmitted intensity. After recording the data points for the transmission curve, the heating is stopped. During the cooling process the ion transmission in forward direction is recorded. At lower temperatures, another measurement is recorded.

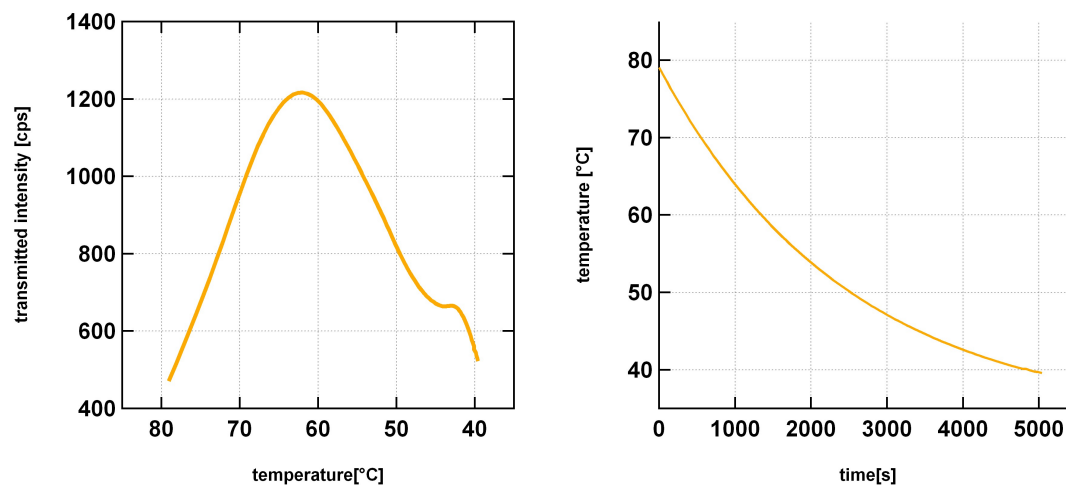


Figure 3.19: **The variation of the transmitted ion intensity in forward direction during the cooling process**

left: The figure shows the increase of the transmitted intensity in forward direction with decreasing temperature until the capillary reaches approximately 60°C. Afterwards the intensity decreases again. The measurements are performed with 4.5 keV Ar^{7+} ions.

right: The temperature decreases exponentially with time.

The curve in figure 3.19 shows the increase of the transmitted ion intensity with decreasing temperature till the capillary reaches circa 60°C. Afterwards the transmitted intensity decreases with decreasing temperature. This still very preliminary results have to be confirmed by further measurement series and are planned for the near future.

An explanation for the initial transmitted intensity increase could be the initiation of the capillary guiding effect. At lower temperatures the effect of Coulomb blocking could still cause the decrease of the transmitted intensity. At lower temperatures or higher incident ion fluxes blocking could become more important.

3.2.3 Ion transmission for different incident ion currents

Another aspect is the dependence of the transmission on the incident beam intensity. Before recording a transmission curve at room temperature, the capillary is heated to 80°C/90°C and the transmitted ion beam is maximized by tilting the capillary. This procedure allows to identify the capillary axis and align it with the beam. Afterwards, the capillary is cooled down and the measurement procedure is started.

Figure 3.20 shows two different transmission curves at room temperature obtained for two different incident ion beam fluxes. The measurements are performed with Ar^{7+} -ions at a kinetic energy of 4.5 keV.

As in the case of straight capillaries, the overall transmission curve becomes ‘wider’ with higher incoming ion flux for tapered capillaries too. There also seems to be a slightly deeper drop for higher intensities. This could be an indication that higher incident ion flux causes the Coulomb blocking to become more influential.

3.2.4 Ion transmission for different ion beam energies

The following section summarises the measurements, which are performed with Ar-ions at different kinetic energies and nearly the same incident ion beam fluxes.

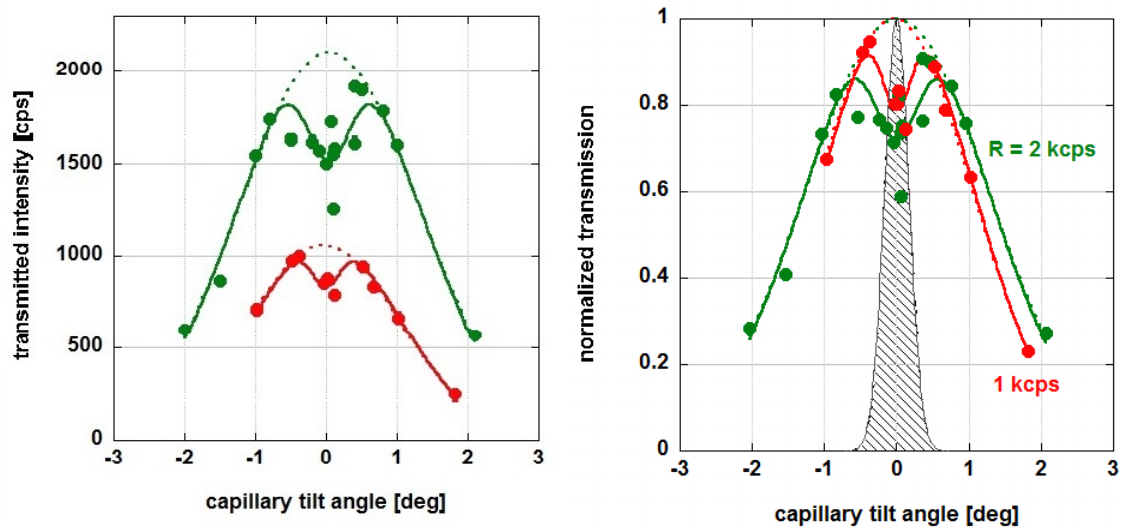


Figure 3.20: **Transmission curves at different incident ion fluxes (Ar^{7+} ; 4.5 keV)**

left: The data points represent the measured and dead-time corrected count rate on the PSD and are fitted according to eq. (3.2) (green: ~ 2 kcps, red: ~ 1 kcps of transmitted ions in forward direction). The dashed line shows the Gaussian function.

right: For comparing the shape of the two different transmission curves, they are normalised relative to the maximum transmission intensity, given by a Gaussian function. The hatched area corresponds to the geometric transmission through the tapered capillary.

Figure 3.21 shows the results of this measurements, performed one time with Ar^{7+} ions at a kinetic energy of 4.5 keV and the other time with Ar^{8+} ions at a kinetic energy of 16 keV. Again the data points are dead-time corrected and fitted according to eq.(3.2).

The measurements confirm that for ions at lower kinetic energies the transmission curve is wider and accordingly the guiding power is stronger. Indeed slower ions need a weaker electrostatic field inside the capillary to be guided through it.

At this point in time, the quality of the acquired data does not allow a firm quantitative

3 Results

comparison of the drop of the transmission curve in forward direction between the two kinetic energies. This will be the subject of further studies with the tapered capillary.

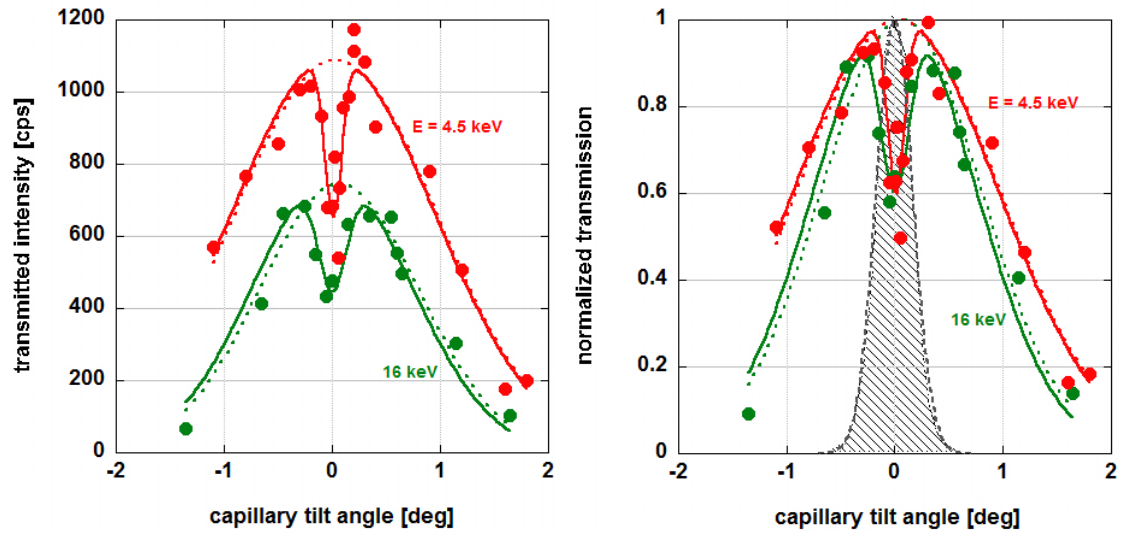


Figure 3.21: Transmission curves at different kinetic energies (red: 4.5 keV, green: 16 keV) of the incident Ar^{7+} - and Ar^{8+} -ions

left: The data points represent the measured and dead-time corrected count rate on the PSD and are fitted according to eq. (3.2). The dashed line shows the Gaussian function.

right: For comparison the transmission curves are normalized relative to the maximum transmission intensity given by the gaussian fit and the hatched area corresponds to the geometric transmission through the tapered capillary.

4 Summary and Outlook

4.1 Summary

Within the scope of this master thesis the guiding effect of single macroscopic glass capillaries in dependency of various physical parameters are studied.

The measurements performed with a single straight capillary mostly confirm the results, which have been obtained in previous investigations with this capillary at TU Wien [82]. In the low temperature region (below room temperature) more systematic experiments are conducted than previously.

Besides the ‘typical character’ of the guiding process, like the charging up period of some hundred seconds and the linear relation between deflection and tilting angle, the key parameters for ion transmission control are investigated in more detail. The charge patch formation of course depends on the electrical conductivity of the capillary’s material, which can be varied by heating or cooling the capillary, and on the incident ion beam flux.

It can be shown that an increase of the electrical conductivity leads to considerable narrowing of the guiding power, until above 75°C the transmission curve approaches a time-independent curve, which corresponds to the geometric transmission through the capillary. This behaviour can be explained by the fact, that at higher temperatures the charge patches are quickly removed and guiding conditions are thus prevented. The same effect is also achieved by decreasing the incident ion beam flux.

Apart from a slight increase of the guiding power at temperatures below room temperature, an erratic movement of the transmitted ions can be observed. The random motion of the ion beam on the detector cover an angular range exceeding by far the geometric opening angle, pointing to changing charge patches near the capillary exit. In comparison, at higher temperatures the beam spot position is stable over hours, showing only small spatial fluctuations.

After the measurements using a straight glass capillary, the investigations of a single tapered glass capillary is started. The constructed tapered capillary holder enables temperature dependent measurements between room temperature and $+90^{\circ}\text{C}$.

First results with the tapered capillary confirm a slight suppression of the transmitted ion beam in forward direction as has been reported in the literature. This dip in of the transmission curve vanishes at higher temperatures. However, it seems that with higher temperatures less ions are transmitted through the capillary in comparison to lower temperatures. This observation leads to the open question, whether the suppression of ion transmission in forward direction is indeed caused by a blocking effect as speculated in literature or simply due to a reduced ion guiding, which is more favorable at slightly asymmetric capillary tilt angles. Preliminary measurements of the transmitted intensity in forward direction during the cooling process suggest, that with decreasing of the temperature the guiding is increased, however, superimposed below 60°C with a kind of blocking of the incident ions. To confirm this hypothesis further measurements are planned.

4.2 Outlook

One of the main tasks for the planned measurements with the tapered capillary in the near future is the verification of the increase/decrease of the transmitted ion intensity in forward direction by changing the electrical conductivity. The ambition is to answer the arisen open question, if the observed drop of the transmitted ions in forward direction

is caused by a blocking or is the result of reduced ion guiding or tentatively also a superimposition of both effects.

Moreover, further measurements are necessary to allow a direct quantitative comparison of depth and width of the drop of the transmission curve in forward direction depending on the capillary temperature (at constant incident ion flux and kinetic energy), on the incident ion flux (at constant temperature and kinetic energy) and on the kinetic energy of the incident ions (at constant temperature and incident ion flux).

It could be also interesting to measure the transmission curve for the tapered capillary at lower temperatures (below room temperature). For this purpose a new sample holder will have to be constructed, which enables a temperature variation by thermic conduction, instead of heat radiation.

A further interesting future project could be the controlling of guiding properties by an external electric field via metal electrodes, fixed on the outer surface of the insulating capillary. It could be investigated how the applied voltages effect the divergence angle of the transmitted and the acceptance angle of the incident ion beam.

From the experimenter's point of view the 'weak spot' of the present setup is the absence of a beam monitor near the capillary entrance, for controlling the stability of the incident ion beam flux. Lots of measurements had to be dropped and repeated several times, because it was difficult to judge if the transmission instabilities, which have sometimes been observed, are caused by the guiding itself or are the result of an unstable incident ion beam. As just mentioned in [82] it is recommended to install a primary beam monitor next to the capillary entrance aperture to get information about the incident ion flux.

Besides the controlling of the stability of the ion beam, this monitoring would also enable a comparing of the incident ion flux with the transmitted ion flux. The current reference apertures can be used for this purpose, however, it was noticed, that when moving the manipulator, sometimes, the previous position of the capillary couldn't be exactly reached again.

Bibliography

- [1] Ratliff L.P., Minniti R., Bard A., Bell E.W., Gillaspay J.D., Parks D., Black A.J. and Whitesides G.M., 'Exposure of self-assembled monolayers to highly charged ions and metastable atoms', *Appl. Phys. Lett.*, **75**, 590 (1999)
- [2] Akcoltekin E., Peters T., Meyer R., Duvenbeck A., Klusmann M., Monnet I., Lebius H. and Schleberger M., 'Creation of multiple nanodots by single ions', *Nature Nanotechnol.*, **2**, 290 (2007)
- [3] El-Said A.S., Heller R., Meissl W., Ritter R., Facsko S., Lemell C., Solleder B., Gebeshuber I.C., Betz G., Toulemonde M., Möller W., Burgdörfer J. and Aumayr F., 'Creation of nanohillocks on CaF₂ surfaces by single slow highly charged ions', *Phys. Rev. Lett.*, **100**, 237601 (2008)
- [4] Heller R., Facsko S., Wilhelm R.A. and Möller W., 'Defect mediated desorption of the KBr(001) surface induced by single highly charged ion impact', *Phys. Rev. Lett.*, **101**, 096102 (2008)
- [5] Schenkel T., Persaud A., Park S.J., Meijer J., Kingsley J.R., McDonald J.W., Holder J.P., Bokor J. and Schneider D.H., 'Single ion implantation for solid state quantum computer development', *J. Vac. Sci. Technol. B*, **20**, 2819 (2002)
- [6] Morton J.J.L., Tyryshkin A.M., Brown R.M., Shankar S., Lovett B.W., Ardavan A., Schenkel T., Haller E.E., Ager J.W. and Lyon S.A., 'Solid-state quantum memory using the ³¹P nuclear spin', *Nature*, **455**, 1085 (2008)
- [7] Iwai Y., Ikeda T., Kojima T.M., Yamazaki Y., Maeshima K., Imamoto N., Kobayashi

- T., Nebiki T., Narusawa T. and Pokhil G.P., 'Ion irradiation in liquid of μm^3 region for cell surgery', *Appl. Phys. Lett.*, **92**, 023509 (2008)
- [8] Tona M., Watanabe H., Takahashi S., Nakamura N., Yoshiyasu N., Sakurai M., Terui T., Mashiko S., Yamada C. and Ohtani S., 'Nano-crater formation on a Si(111)-(7 \times 7) surface by slow highly charged ion-impact', *Surf. Sci.*, **601**, 723 (2007)
- [9] Tona M., Fujita Y., Yamada C. and Ohtani S., 'Electronic interaction of individual slow highly charged ions with TiO₂(110)', *Phys. Rev. B*, **77**, 155427 (2008)
- [10] Aumayr F., El-Said A.S. and Meissl W., 'Nano-sized surface modifications induced by the impact of slow highly charged ions – A first review', *Nucl. Instrum. Methods. Phys. Res., Sect. B*, **266**, 2729 (2008)
- [11] Stolterfoht N., Bremer J.H., Hoffmann V., Hellhammer R., Fink D., Petrov A. and Sulik B., 'Transmission of 3 keV Ne⁷⁺ ions through nanocapillaries etched in polymer foils: Evidence for capillary guiding', *Phys. Rev. Lett.*, **88**, 133201 (2002)
- [12] Burgdörfer J., Lerner P. and Meyer F.W., 'Above-surface neutralization of highly charged ions: The classical over-the-barrier model', *Phys. Rev. A*, **44**, 5674 (1991)
- [13] Yamazaki Y., Ninomiya S., Koike F., Masuda H., Azuma T., Komaki K., Kuroki K. and Sekiguchi M., 'Stabilized Hollow Atoms (Ions) Produced with Multiply Charged Ions Passed through Microcapillaries', *J. Phys. Soc. Jpn.*, **65**, 1199 (1996)
- [14] Yamazaki Y., 'Production of hollow atoms (ions) in HCI-surface collision', *Phys. Scr.*, **73**, 293 (1997)
- [15] Ninomiya S., Yamazaki Y., Koike F., Masuda H., Azuma T., Komaki K., Kuroki K. and Sekiguchi M., 'Stabilized hollow ions extracted in vacuum', *Phys. Rev. Lett.*, **78**, 4557 (1997)
- [16] Yamazaki Y., 'A microcapillary target as a metastable hollow ion source', *Nucl. Instrum. Methods Phys. Res., Sect. B*, **193**, 516 (2002)

- [17] Morishita Y., Kanai Y., Ando K., Hutton R., Brage T., Torii H.A., Komaki K., Masuda H., Ishii K. and Rosmej F.B., 'Visible light spectroscopy of Ar 6^+ ions in high Rydberg states produced with a microcapillary target', *Nucl. Instr. and Meth. B*, **205**, 758 (2003)
- [18] Tókési K., Wirtz L., Lemell C. and Burgdörfer J., 'Transmission of highly charged ions through microcapillaries', *Nucl. Instrum. Methods Phys. Res., Sect. B*, **164**, 504 (2000)
- [19] Donets E., 'Electron beam ion sources and associated physics at JINR', *Nucl. Instrum. Methods Phys. Res., Sect. B*, **9**, 522 (1985)
- [20] Briand J.P., de Billy L., Charles P., Essabaa S., Briand P., Geller R., Desclaux J.P., Bliman S. and Ristori C., 'Production of hollow atoms by the excitation of highly charged ions in interaction with a metallic surface', *Phys. Rev. Lett.*, **65**, 159 (1990)
- [21] Aumayr F. and Winter H., *Comments At. Mol. Phys.*, **29**, 275 (1994)
- [22] Arnau A., Aumayr F., Echenique P.M., Grether M., Heiland W., Limburg J., Morgenstern R., Roncin P., Schippers S. Schuch R., Stolterfoht N., Varga P., Zouros T.J.M. and Winter H.P., 'Interaction of slow multicharged ions with solid surfaces', *Surf. Sci. Rep.*, **27**, 113 (1997)
- [23] Limburg J., Schippers S., Hughes I., Hoekstra R., Morgenstern R., Hustedt S., Hatke N. and Heiland W., 'Probing hollow atom states formed during impact of highly charged ions on surfaces: N $^{6,7+}$ and O $^{7+}$ on Al(110) and Si(100)', *Nucl. Instrum. Methods Phys. Res., Sect. B*, **98**, 436 (1995)
- [24] Grether M., Spieler A., Niemann D. and Stolterfoht N., 'Formation and filling of hollow Ne atoms below an Al surface', *Phys. Rev. A*, **56**, 3794 (1997)
- [25] Yamazaki Y., 'Interaction of slow highly-charged ions with metals and insulators', *Nucl. Instrum. Methods Phys. Res., Sect. B*, **258**, 139 (2007)

- [26] Schiessl K., Palfinger W., Tókési K., Nowotny H., Lemell C. and Burgdörfer J., ‘Simulation of guiding of multiply charged projectiles through insulating capillaries’, *Phys. Rev. A*, **72**, 062902 (2005)
- [27] Schiessl K., Palfinger W., Lemell C. and Burgdörfer J., ‘Simulation of guiding of highly charged projectiles through insulating nanocapillaries’, *Nucl. Instrum. Methods Phys. Res., Sect. B*, **232**, 228 (2005)
- [28] Schiessl K., Palfinger W., Tókési K., Nowotny H., Lemell C. and Burgdörfer J., ‘Simulation of ion guiding through insulating capillaries: Effects of inter-capillary interaction’, *Nucl. Instrum. Methods Phys. Res., Sect. B*, **258**, 150 (2007)
- [29] Schiessl K., Lemell C., Tókési K. and Burgdörfer J., ‘Simulation of charged particle guiding through insulating nanocapillaries’, *J. Phys. Conf. Ser.*, **194**, 012069 (2009)
- [30] Schiessl K., Lemell C., Tókési K. and Burgdörfer J., ‘Energy dependence of ion guiding through nanocapillaries’, *J. Phys. Conf. Ser.*, **163**, 012081 (2009)
- [31] Lemell C., Schiessl K., Nowotny H. and Burgdörfer J., ‘Simulation of heavy-ion guiding in insulators’, *Nucl. Instrum. Methods Phys. Res., Sect. B*, **256**, 66 (2007)
- [32] Gunacker P., *Simulating transmission behavior of highly charged ions through microscopic capillaries*, Bachelor Thesis, TU Wien, ITP (2012)
- [33] Stolterfoht N., Hoffmann V., Hellhammer R., Pei Z., Fink D., Petrov A. and Sulik B., ‘Guided transmission of 3 keV Ne^{7+} ions through nanocapillaries etched in a PET polymer’, *Nucl. Instrum. Methods Phys. Res., Sect. B*, **203**, 246 (2003)
- [34] Stolterfoht N., Hellhammer R., Pešić Z.D., Hoffmann V., Bundesmann J., Petrov A., Fink D., Sulik B., Shah M., Dunn K., Pedregosa J. and McCullough R.W., ‘Time evolution of ion guiding through nanocapillaries in a PET polymer’, *Nucl. Instrum. Methods Phys. Res., Sect. B*, **225**, 169 (2004)
- [35] Stolterfoht N., ‘Guided transmission of Ne^{7+} ions through nanocapillaries in PET: dependence on the tilt angle’, *Vacuum*, **73**, 31 (2004)

- [36] Stolterfoht N., Hellhammer R., Sobocinski P., Pešić Z.D., Bundesmann J., Sulik B., Shah M.B., Dunn K., Pedregosa J. and McCullough R.W., ‘Guiding of slow neon and molecular hydrogen ions through nanocapillaries in PET’, *Nucl. Instrum. Methods Phys. Res., Sect. B*, **235**, 460 (2005)
- [37] Hellhammer R., Sobocinski P., Pešić Z., Bundesmann J., Fink D. and Stolterfoht N., ‘Interaction of slow highly charged ions with the inner surface of nanocapillaries’, *Nucl. Instrum. Methods Phys. Res., Sect. B*, **232**, 235 (2005)
- [38] Hellhammer R., Pešić Z.D., Sobocinski P., Fink D., Bundesmann J. and Stolterfoht N., ‘Guided transmission of highly charged ions through nanocapillaries in PET: Study of the energy dependence’, *Nucl. Instrum. Methods Phys. Res., Sect. B*, **233**, 213 (2005)
- [39] Fürsatz M., Meissl W., Pleschko S., Gebeshuber I.C., Stolterfoht N., Winter H.P. and Aumayr F., ‘Charging and discharging of nano-capillaries during ion guiding of multiply charged projectiles’, *J. Phys. Conf. Ser.*, **58**, 319 (2007)
- [40] Kreller M., Zschornack G. and Kentsch U., ‘Guiding of Argon ions through PET nano capillary foils’, *J. Phys. Conf. Ser.*, **163**, 012090 (2009)
- [41] Viktor G., Kumar R.T.R., Pešić Z.D., Stolterfoht N. and Schuch R., ‘Guiding of slow highly charged ions by nanocapillaries in PET’, *Nucl. Instrum. Methods Phys. Res., Sect. B*, **233**, 218 (2005)
- [42] Kumar R.T.R., Badel X., Viktor G., Linnros J. and Schuch R., ‘Fabrication of silicon dioxide nanocapillary arrays for guiding highly charged ions’, *Nanotechnology*, **16**, 1697 (2005)
- [43] Sahana M.B., Skog P., Viktor G., Kumar R.T.R. and Schuch R., ‘Guiding of highly charged ions by highly ordered SiO₂ nanocapillaries’, *Phys. Rev. A*, **73**, 040901 (2006)
- [44] Skog P., Zhang H.Q. and Schuch R., ‘Evidence of Sequentially Formed Charge Patches Guiding Ions through Nanocapillaries’, *Phys. Rev. Lett.*, **101**, 223202 (2008)

- [45] Zhang H.Q., Skog P. and Schuch R., ‘Dynamics of guiding highly charged ions through SiO₂ nanocapillaries’, *Phys. Rev. A*, **82**, 052901 (2010)
- [46] Allen F., Persaud A., Park S., Minor A., Sakurai M., Schneider D. and Schenkel T., ‘Transport of multiply and highly charged ions through nanoscale apertures in silicon nitride membranes’, *Nucl. Instrum. Methods Phys. Res., Sect. B*, **244**, 323 (2006)
- [47] Mátéfi-Tempfli S., Mátéfi-Tempfli M., Piraux L., Juhász Z., Biri S., Fekete E., Iván I., Gáll F., Sulik B., Víkor G., Pálinkás J. and Stolterfoht N., ‘Guided transmission of slow Ne⁶⁺ ions through the nanochannels of highly ordered anodic alumina’, *Nanotechnology*, **17**, 3915 (2006)
- [48] Skog P., Soroka I.L., Johansson A. and Schuch R., ‘Guiding of highly charged ions through Al₂O₃ nano-capillaries’, *Nucl. Instrum. Methods Phys. Res., Sect. B*, **258**, 145 (2007)
- [49] Juhász Z., Sulik B., Biri S., Iván I., Tókési K., Fekete E., Mátéfi-Tempfli S., Mátéfi-Tempfli M., Víkor G., Takács E. and Pálinkás J., ‘Ion guiding in alumina capillaries: MCP images of the transmitted ions’, *Nucl. Instrum. Methods Phys. Res., Sect. B*, **267**, 321 (2009)
- [50] Krause H., Vane C. and Meyer F., ‘Ions transmitted through an anodic nanocapillary array’, *Phys. Rev. A*, **75**, 042901 (2007)
- [51] Wang H., Chen L., Lv X., Zhou C., Jia J., Zhou P., Shao J., Ji M. and Chen X., ‘Transmission of 16 keV Cu⁻ ions through Al₂O₃ nano-capillaries’, *Nucl. Instrum. Methods Phys. Res., Sect. B*, **286**, 351 (2012)
- [52] Stolterfoht N., Hellhammer R., Bundesmann J. and Fink D., ‘Scaling laws for guiding of highly charged ions through nanocapillaries in an insulating polymer’, *Phys. Rev. A*, **77**, 032905 (2008)
- [53] Stolterfoht N., Hellhammer R., Fink D., Sulik B., Juhász Z., Bodewits E., Dang

- H.M. and Hoekstra R., ‘Dynamic properties of ion guiding through nanocapillaries in an insulating polymer’, *Phys. Rev. A*, **79**, 022901 (2009)
- [54] Hellhammer R., Bundesmann J., Fink D. and Stolterfoht N., ‘Scaling laws for guiding of highly charged ions through nanocapillaries in insulating PET’, *Nucl. Instrum. Methods Phys. Res., Sect. B*, **258**, 159 (2007)
- [55] Stolterfoht N., Hellhammer R., Juhasz Z., Sulik B., Bodewits E., Dang H.M. and Hoekstra R., ‘Guided transmission of 3-keV Ne^{7+} ions through nanocapillaries in insulating polymers: Dependence on the capillary diameter’, *Phys. Rev. A*, **82**, 052902 (2010)
- [56] Ikeda T., Kanai Y., Kojima T.M., Iwai Y., Kambara T., Yamazaki Y., Hoshino M., Nebiki T. and Narusawa T., ‘Production of a microbeam of slow highly charged ions with a tapered glass capillary’, *Appl. Phys. Lett.*, **89**, 163502 (2006)
- [57] Bereczky R.J., Kowarik G., Aumayr F. and Tőkési K., ‘Transmission of 4.5 keV Ar^{9+} ions through a single glass macro-capillary’, *Nucl. Instrum. Methods Phys. Res., Sect. B*, **267**, 317 (2009)
- [58] Kowarik G., Bereczky R.J., Aumayr F. and Tőkési K., ‘Production of a microbeam of slow highly charged ions with a single microscopic glass capillary’, *Nucl. Instrum. Methods Phys. Res., Sect. B*, **267**, 2277 (2009)
- [59] Skog P., Zhang H.Q., Akram N., Soroka I.L., Trautmann C. and Schuch R., ‘Guiding of slow Ne^{7+} -ions through insulating nano-capillaries of various geometrical cross-sections’, *J. Phys. Conf. Ser.*, **194**, 132030 (2009)
- [60] Zhang H.Q., Akram N., Soroka I., Trautmann C. and Schuch R., ‘Transmission of highly charged ions through mica nanocapillaries of rhombic cross section’, *Phys. Rev. A*, **86** (2012)
- [61] Zhang H.Q., Akram N., Skog P., Soroka I., Trautmann C. and Schuch R., ‘Tailoring of keV-Ion Beams by Image Charge when Transmitting through Rhombic and Rectangular Shaped Nanocapillaries’, *Phys. Rev. Lett.*, **108**, 193202 (2012)

- [62] Kojima T.M., Ikeda T., Kanai Y., Yamazaki Y. and Esaulov V.A., ‘Ion beam guiding with straight and curved Teflon tubes’, *J. Phys. D: Appl. Phys.*, **44**, 355201 (2011)
- [63] Pokhil G.P., Vokhmyanina K.A., Zhilyakov L.A., Ikeda T., Kanai Y., Iwai Y., Kojima T.M. and Yamazaki Y., ‘Ion guiding through a flat insulating channel’, *Bulletin of the Russian Academy of Sciences: Physics*, **72**, 638 (2008)
- [64] Pokhil G.P., Vokhmyanina K.A. and Mironchik A.I., ‘Model of ion beam guiding using a flat capillary’, *Journal of Surface Investigation. X-ray, Synchrotron and Neutron Techniques*, **3**, 326 (2009)
- [65] Ikeda T., Kanai Y., Kojima T., Iwai Y., Kanazawa Y., Hoshino Y., Kobayashi T., Pokhil G. and Yamazaki Y., ‘Focusing of charged particle beams with various glass-made optics’, *J. Phys. Conf. Ser.*, **88**, 012031 (2007)
- [66] Milosavljević A., Víkor G., Pešić Z., Kolarž P., Šević D., Marinković B., Mátéfi-Tempfli S., Mátéfi-Tempfli M. and Piraux L., ‘Guiding of low-energy electrons by highly ordered Al_2O_3 nanocapillaries’, *Phys. Rev. A*, **75**, 030901 (2007)
- [67] Das S., Dassanayake B.S., Winkworth M., Baran J.L., Stolterfoht N. and Tanis J.A., ‘Inelastic guiding of electrons in polymer nanocapillaries’, *Phys. Rev. A*, **76**, 042716 (2007)
- [68] Dassanayake B.S., Das S., Bereczky R.J., Tókési K. and Tanis J.A., ‘Energy dependence of electron transmission through a single glass macrocapillary’, *Phys. Rev. A*, **81**, 020701 (2010)
- [69] Dassanayake B.S., Das S., Ayyad A., Bereczky R.J., Tókési K. and Tanis J.A., ‘Charge evolution and energy loss associated with electron transmission through a macroscopic single glass capillary’, *Nucl. Instrum. Methods Phys. Res., Sect. B*, **269**, 1243 (2011)
- [70] Dassanayake B., Bereczky R., Das S., Ayyad A., Tókési K. and Tanis J., ‘Time

- evolution of electron transmission through a single glass macrocapillary: Charge build-up, sudden discharge, and recovery', *Phys. Rev. A*, **83**, 012707 (2011)
- [71] Milosavljević A.R., Jureta J., Víkor G., Pešić Z.D., Šević D., Mátéfi-Tempfli M., Mátéfi-Tempfli S. and Marinković B.P., 'Low-energy electron transmission through high aspect ratio Al_2O_3 nanocapillaries', *EPL*, **86**, 23001 (2009)
- [72] Schiessl K., Tókési K., Solleder B., Lemell C. and Burgdörfer J., 'Electron Guiding through Insulating Nanocapillaries', *Phys. Rev. Lett.*, **102**, 163201 (2009)
- [73] Nebiki T., Sekiba D., Yonemura H., Wilde M., Ogura S., Yamashita H., Matsumoto M., Fukutani K., Okano T. and Kasagi J., 'Taper angle dependence of the focusing effect of high energy heavy ion beams by glass capillaries', *Nucl. Instrum. Methods Phys. Res., Sect. B*, **266**, 1324 (2008)
- [74] Chen L., Guo Y., Jia J., Zhang H., Cui Y., Shao J., Yin Y., Qiu X., Lv X., Sun G., Wang J., Chen Y., Xi F. and Chen X., 'Absence of a guiding effect and charge transfer in the interaction of keV-energy negative ions with Al_2O_3 nanocapillaries', *Phys. Rev. A*, **84**, 032901 (2011)
- [75] Chen L., Lv X., Jia J., Ji M., Zhou P., Sun G., Wang J., Chen Y., Xi F., Cui Y., Shao J., Qiu X., Guo Y. and Chen X., 'Charge exchange of keV O^- ions transmitted through Al_2O_3 nano-capillaries', *J. Phys. B: At. Mol. Opt. Phys.*, **44**, 045203 (2011)
- [76] Feng D., Shao J., Zhao L., Ji M., Zou X., Wang G., Ma Y., Zhou W., Zhou H., Li Y., Zhou M. and Chen X., 'Dynamic guiding process of 10-keV O^- ions transmitting through Al_2O_3 nanocapillaries', *Phys. Rev. A*, **85**, 064901 (2012)
- [77] Sun G., Chen X., Wang J., Chen Y., Xu J., Zhou C., Shao J., Cui Y., Ding B., Yin Y., Wang X., Lou F., Lv X., Qiu X., Jia J., Chen L., Xi F., Chen Z., Li L. and Liu Z., 'Interaction of 18-keV O^- ions with Al_2O_3 nanocapillaries', *Phys. Rev. A*, **79**, 052902 (2009)
- [78] DuBois R.D. and Tókési K., 'Can positrons be guided by insulating capillaries?' *Nucl. Instrum. Methods Phys. Res., Sect. B*, **279**, 186 (2012)

- [79] Oshima N., Iwai Y., Kojima T.M., Ikeda T., Kanazawa Y., Hoshino M., Suzuki R. and Yamazaki Y., ‘Guiding of a Slow Positron Beam with a Glass Capillary’, *Positron and Positronium Chemistry*, **607**, 263 (2009)
- [80] Kojima T.M., Tomono D., Ikeda T., Ishida K., Iwai Y., Iwasaki M., Matsuda Y., Matsuzaki T. and Yamazaki Y., ‘Density Enhancement of Muon Beams with Tapered Glass Tubes’, *J. Phys. Soc. Jpn.*, **76**, 093501 (2007)
- [81] Tomono D., Kojima T.M., Ishida K., Ikeda T., Iwai Y., Tokuda M., Kanazawa Y., Matsuda Y., Matsuzaki T., Iwasaki M. and Yamazaki Y., ‘Focusing Effect of MeV Muon Beam with a Tapered Capillary Method’, *J. Phys. Soc. Jpn.*, **80**, 044501 (2011)
- [82] Kowarik G., ‘The interaction of highly charged ions with insulating matter: capillary guiding and related phenomena’, Ph.D. thesis, TU Wien, IAP (2011)
- [83] Kowarik G., Bereczky R., Ladinig F., Schrempf D., Lemell C., Burgdörfer J., Tókési K. and Aumayr F., ‘Temperature control of ion guiding through insulating capillaries’, *arXiv:1109.3953 [cond-mat.other]* (2011)
- [84] Cassimi A., Maunoury L., Muranaka T., Huber B., Dey K.R., Lebius H., Lelievre D., Ramillon J.M., Been T., Ikeda T., Kanai Y., Kojima T.M., Iwai Y., Yamazaki Y., Khemliche H., Bundaleski N. and Roncin P., ‘Imaging dynamics of charge-auto-organisation in glass capillaries’, *Nucl. Instrum. Methods Phys. Res., Sect. B*, **267**, 674 (2009)
- [85] Kreller M., Zschornack G. and Kentsch U., ‘Guiding of argon ions through a tapered glass capillary’, *Nucl. Instrum. Methods Phys. Res., Sect. B*, **269**, 1032 (2011)
- [86] Nakayama R., Tona M., Nakamura N., Watanabe H., Yoshiyasu N., Yamada C., Yamazaki A., Ohtani S. and Sakurai M., ‘Guiding and blocking of highly charged ions through a single glass capillary’, *Nucl. Instrum. Methods Phys. Res., Sect. B*, **267**, 2381 (2009)

- [87] Nebiki T., Kabir M.H. and Narusawa T., ‘In-air PIXE analysis by means of glass capillary optics’, *Nucl. Instrum. Methods Phys. Res., Sect. B*, **249**, 226 (2006)
- [88] Hasegawa J., Shiba S., Fukuda H. and Oguri Y., ‘A compact micro-beam system using a tapered glass capillary for proton-induced X-ray radiography’, *Nucl. Instrum. Methods Phys. Res., Sect. B*, **266**, 2125 (2008)
- [89] Hasegawa J., Jaiyen S., Polee C. and Oguri Y., ‘Development of a micro-PIXE system using tapered glass capillary optics’, *Nucl. Instrum. Methods Phys. Res., Sect. B*, **269**, 3087 (2011)
- [90] Simon M.J., Döbeli M., Müller A.M. and Synal H.A., ‘In-air STIM with a capillary microprobe’, *Nucl. Instrum. Methods Phys. Res., Sect. B*, **273**, 237 (2012)
- [91] Sekiba D., Yonemura H., Nebiki T., Wilde M., Ogura S., Yamashita H., Matsumoto M., Kasagi J., Iwamura Y., Itoh T., Matsuzaki H., Narusawa T. and Fukutani K., ‘Development of micro-beam NRA for 3D-mapping of hydrogen distribution in solids: Application of tapered glass capillary to 6 MeV ^{15}N ion’, *Nucl. Instrum. Methods Phys. Res., Sect. B*, **266**, 4027–4036 (2008)
- [92] Kobayashi T., Miyamoto S., Ikeda T., Kojima T.M., Ogiwara K. and Yamazaki Y., ‘Surface modification of polymers by ion irradiation at the solid-liquid interface’, *Nucl. Instrum. Methods Phys. Res., Sect. B*, **272**, 405 (2012)
- [93] Iwai Y., Ikeda T., Kojima T.M., Yamazaki Y., Maeshima K., Imamoto N., Kobayashi T., Nebiki T., Narusawa T. and Pokhil G.P., ‘Ion irradiation in liquid of μm^3 region for cell surgery’, *Appl. Phys. Lett.*, **92**, 023509 (2008)
- [94] Ikeda T., Kanai Y., Iwai Y., Kojima T.M., Maeshima K., Meissl W., Kobayashi T., Nebiki T., Miyamoto S., Pokhil G.P., Narusawa T., Imamoto N. and Yamazaki Y., ‘Glass capillary optics for producing nanometer sized beams and its applications’, *Surface and Coatings Technology*, **206**, 859 (2011)
- [95] Naderer P., ‘Erosion of tungsten surfaces by nitrogen ions’, Master’s thesis, TU Wien, IAP (2011)

- [96] Galutschek E., ‘Development of a 14.5 GHz All-Permanent Magnet Multicharged ECR Ion Source for Remote Operation’, Ph.D. thesis, TU Wien, IAP (2005)
- [97] Iskratsch K., ‘New Design of an Ion Source Control Software and Investigations of Ion-Induced Electron Emission from LiF’, Master’s thesis, TU Wien, IAP (2009)
- [98] Gruber E., *Assembly of the new vacuum system*, Project report, TU Wien, IAP (2011)
- [99] Fuchs-Fuchs A., *PLC-ion-guiding-facility (in progress)*, Project report, TU Wien, IAP (2012)
- [100] ‘RoentDek’, (2011), URL <http://www.roentdek.com>.
- [101] ‘KMax’, (2008), URL <http://www.sparrowcorp.com/>.
- [102] ‘I. Pro. IGOR Pro 6.0.’ (2010), URL <http://www.wavemetrics.com>.
- [103] Berezky R.J., Kowarik G., Lemaignan C., Macè A. and Ladinig F., Raab R., Aumayr F., Tökési K., McDaniel F.D. and Doyle B.L., ‘Guiding Of Slow Highly Charged Ions Through A Single Mesoscopic Glass Capillary’, *AIP Conference Proceedings*, **1336**, 119 (2011)
- [104] Hischenhuber P., *Konstruktion und Entwicklung eines Targethalters für Messungen mit verjüngten Glaskapillaren*, Bachelor Thesis, TU Wien, IAP (2011)
- [105] Waclawek J., *Messung der Leitfähigkeit von Duran Borosilikatglas*, Bachelor Thesis, TU Wien, IAP (2010)

Danksagung

Abschließend möchte ich mich noch bei all jenen Menschen bedanken, die mich bei der Erarbeitung meiner Masterarbeit unterstützt haben.

Dabei geht ein sehr großer Dank an meinen Betreuer Prof. Friedrich Aumayr, der mir durch seine fachliche Kompetenz immer wieder bei physikalischen Fragestellungen weiterhelfen konnte und Anregungen für die Durchführung des Experiments gab. Er ermöglichte mir erste Erfahrungen in der Wissenschaftswelt zu sammeln und zeigte stets großes Interesse am Vorangehen der Arbeit. Sein offener und persönlicher Umgang mit Studenten trägt zu einer sehr angenehmen Arbeitsgruppenatmosphäre bei und ermuntert Vertrauen im selbstständigen Arbeiten zu bekommen. Besonders bedanken möchte ich mich auch dafür, dass ich jederzeit mit verschiedensten Anliegen an der Bürotür anklopfen konnte und Gehör fand.

Ein weiteres großes Dankeschön geht an B.Sc. Paul Berlinger, der Elektronikfachmann des Instituts, für seine schnellen und gewissenhaften Reparaturen. Weiter möchte ich mich auch bei den Mitarbeitern der Werkstätte, Wolfgang Beck, Herbert Schmidt und Rainer Gärtner für die Anfertigung und Verbesserungsvorschläge des Probenhalters bedanken.

Ein großer Dank gilt auch der Arbeitsgruppe für Atom- und Plasmaphysik für die angenehme familiäre Atmosphäre. Besonders bedanken möchte ich mich bei Dr. Gregor Kowarik, der mich bereits während der Bachelorarbeit, während einer Projektarbeit zum Umbau der Vakuumanlage im Augustinlabor und am Beginn meiner Masterarbeit betreut hat. Ich konnte durch dein großes Wissen und deine langjährige Laborerfahrung viel dazulernen, und die Freude und der Einsatz, mit denen du deine Arbeiten ausgeführt hast, waren für mich stets ein Vorbild. Auch außerhalb des universitären Betriebes bist du für mich inzwischen ein sehr guter Freund und Gesprächspartner geworden. Du zeigst stets große Offenheit und Diskutierfreudigkeit und erfrischt durch deine unkonventionelle

Denkart, welche auch beim Arbeiten im Labor immer wieder hilfreich sein konnte.

Nachdem Gregor nach Abschluss seiner Dissertation die Arbeitsgruppe verlassen hat, hat Dipl. Ing. Katharina Dobes die Leitung des Augustinlabors übernommen und wurde zur ersten Ansprechperson für jegliches Problem. Auch dir Kathi möchte ich für die Unterstützung und Hilfsbereitschaft in den letzten Monaten danken. Du hast dir für meine Anliegen immer wieder Zeit genommen und mir versucht bei verschiedensten Problemen zu helfen.

Ein weiteres Dankeschön geht an Alexander Fuchs-Fuchs, der als Projektstudent an der Steuerung der Vakuumanalge arbeitete. Der anfangs unterschätzte Arbeitsaufwand und dein Hang zum Perfektionismus ließen dich länger im Labor bleiben als du ursprünglich geplant hast. Dadurch hatte ich die Möglichkeit dich besser kennenzulernen, und du wurdest für mich einer der wichtigsten Bezugspersonen im letzten Jahr. Es war immer wieder schön mit dir über 'Gott und die Welt' zu reden und natürlich danke ich dir für deine Geduld, wenn ich wieder mal mit meinen Computerproblemen zu dir kam.

Im Weiteren möchte ich mich bei meinen Projektstudenten Peter Hischenhuber und Stefan Wampl bedanken, die mir bei der Planung des Probenhalters und den durchgeführten Messungen zuverlässig geholfen haben.

Zu guter Letzt möchte ich noch meiner Familie für die Unterstützung über all die Jahre und für die Rücksichtnahme und Fürsorge trotz familiärer Schwierigkeiten in den letzten Monaten danken. Meiner Mama möchte ich dafür danken, dass sie mir das Studium ermöglicht hat und stets großes Vertrauen in mich setzte. Meine Schwestern haben all die Hoch und Tiefs mit mir miterlebt und mich immer wieder zum Weitermachen ermutigt. Besonders bei dir, Steffi möchte ich mich für deine einfühlsamen Ratschläge und Worte bedanken.